Received: 8 January 2021 | Revised: 16 June 2021 | Accepted: 16 August 2021

DOI: 10.1002/cne.25234

RESEARCH ARTICLE

JCN RESEARCH IN SYSTEMS NEUROSCIENCE THE JOURNAL OF COMPARATIVE NEUROLOGY WILEY

Comparative description of the mRNA expression profile of Na^+/K^+-ATPase isoforms in adult mouse nervous system

Song Jiao[1] | **Kory Johnson**[2] | **Cristina Moreno**[1] | **Sho Yano**[1] | **Miguel Holmgren**[1]

[1]Molecular Neurophysiology Section, National Institute of Neurological Disorders and Stroke, National Institutes of Health, Bethesda, Maryland, USA

[2]Bioinformatics Section, National Institute of Neurological Disorders and Stroke, National Institutes of Health, Bethesda, Maryland, USA

Correspondence
Miguel Holmgren, Molecular Neurophysiology Section, National Institute of Neurological Disorders and Stroke, National Institutes of Health, Bethesda, MD 20892, USA.
Email: holmgren@ninds.nih.gov

Funding information
National Institute of Neurological Disorders and Stroke, Grant/Award Number: NS002993

Abstract

Mutations in genes encoding Na^+/K^+-ATPase α1, α2, and α3 subunits cause a wide range of disabling neurological disorders, and dysfunction of Na^+/K^+-ATPase may contribute to neuronal injury in stroke and dementia. To better understand the pathogenesis of these diseases, it is important to determine the expression patterns of the different Na^+/K^+-ATPase subunits within the brain and among specific cell types. Using two available scRNA-Seq databases from the adult mouse nervous system, we examined the mRNA expression patterns of the different isoforms of the Na^+/K^+-ATPase α, β and *Fxyd* subunits at the single-cell level among brain regions and various neuronal populations. We subsequently identified specific types of neurons enriched with transcripts for α1 and α3 isoforms and elaborated how α3-expressing neuronal populations govern cerebellar neuronal circuits. We further analyzed the co-expression network for α1 and α3 isoforms, highlighting the genes that positively correlated with α1 and α3 expression. The top 10 genes for α1 were *Chn2*, *Hpcal1*, *Nrgn*, *Neurod1*, *Selm*, *Kcnc1*, *Snrk*, *Snap25*, *Ckb* and *Ccndbp1* and for α3 were *Sorcs3*, *Eml5*, *Neurod2*, *Ckb*, *Tbc1d4*, *Ptprz1*, *Pvrl1*, *Kirrel3*, *Pvalb*, and *Asic2*.

KEYWORDS
expression profile, mouse brain, Na/K ATPase

1 | INTRODUCTION

The Na^+/K^+-ATPase is an essential transmembrane protein in most eukaryotic cells. It maintains the concentration gradients of Na^+ and K^+ across the cell membrane, which are used for a variety of cell maintenance processes. In neurons, these gradients are also needed for action potential generation and excitability. Structurally, the Na^+/K^+-ATPase is a complex of three protein subunits, namely the catalytic α subunit, the auxiliary β subunit, and the small regulatory subunit (Arystarkhova et al., 1999; Jaisser et al., 1992; Lutsenko & Kaplan, 1993; Mercer et al., 1993; Morth et al., 2007; Schneider et al., 1985; Shinoda et al., 2009; Shull, Greeb, & Lingrel, 1986; Shull, Lane, & Lingrel, 1986). Four α subunit isoforms are expressed in mammalian cells in a spatiotemporally regulated manner (Blanco & Mercer, 1998; Clausen et al., 2017; Lingrel et al., 1990). Within the nervous system, the α1 isoform is ubiquitously expressed, while α2 and α3 isoforms are predominantly observed in glia and neurons, respectively (Bottger et al., 2011; Cameron et al., 1994; Dobretsov et al., 2019; Edwards et al., 2013; Murata et al., 2020; Richards et al., 2007; Sweadner, 1991). The α4 isoform expresses exclusively in testis and is essential for sperm motility and fertility (Jimenez, McDermott, Sanchez, & Blanco, 2011a; Jimenez, Sanchez, et al., 2011; Shamraj & Lingrel, 1994). Similarly, the three β isoforms express differently among nervous tissues and cells, yet β1 appears to be the predominant isoform among neurons (Arystarkhova & Sweadner, 1997; Clausen et al., 2017; Lecuona et al., 1996; Peng et al., 1997; Zlokovic et al., 1993). Even though there are seven small regulatory subunit isoforms, *Fxyd6* and *Fxyd7* are the major isoforms in CNS neurons (Beguin et al., 2002; Delprat et al., 2007; Geering, 2005; Kadowaki et al., 2004; Sweadner & Rael, 2000).

Given the importance of Na^+/K^+-ATPase in electrically excitable tissues, it is not surprising that mutations of α1, α2, and α3, the three

α-subunit isoforms expressed in the nervous system, cause severe neurological disorders. Mutations of *ATP1A1*, encoding α1, cause forms of epilepsy, Charcot–Marie–Tooth disease, and hereditary spastic paraplegia (He et al., 2019; Lassuthova et al., 2018; Schlingmann et al., 2018; Stregapede et al., 2020). Consistent with its expression in astrocytes, mutations of *ATP1A2* (α2) cause familial hemiplegic migraine type 2, thought to involve inadequate astrocyte clearance of extracellular K^+ and neurotransmitters (Gritz & Radcliffe, 2013; Vanmolkot et al., 2006). Mutations in *ATP1A3* (α3) cause many rare neurological diseases involving various combinations of symptoms, such as dystonia, hemiplegia, cerebellar ataxia, epilepsy, and intellectual disability. These include rapid-onset dystonia-parkinsonism (RDP) (Anselm et al., 2009; Brashear et al., 2007; de Carvalho Aguiar et al., 2004; Lee et al., 2007; McKeon et al., 2007; Rodacker et al., 2006), alternating hemiplegia of childhood (AHC) (Heinzen et al., 2012; Hoei-Hansen et al., 2014; Panagiotakaki et al., 2010; Rosewich et al., 2012; Yang et al., 2014), cerebellar ataxia, areflexia, pes cavus, optic atrophy, and sensorineural hearing loss (CAPOS) syndrome (Demos et al., 2014; Heimer et al., 2015; Maas et al., 2016), and catastrophic early life epilepsy, episodic apnea, and postnatal microcephaly (Paciorkowski et al., 2015). The majority of patients with AHC have causative heterozygous α3 mutations (>74%) (Heinzen et al., 2012). Moreover, transgenic mice with heterozygous knockout of α3 (DeAndrade et al., 2011; Ikeda et al., 2013; Ikeda et al., 2017; Moseley et al., 2007), or with α3-point mutations (D801Y, D801N or I810N) which impair enzymatic activity (Clapcote et al., 2009; Hunanyan et al., 2015; Isaksen et al., 2017; Kirshenbaum, Clapcote, et al., 2011; Kirshenbaum, Saltzman, et al., 2011), manifest disease symptoms similar to those in humans. In addition to these genetic disorders, dysfunction of Na^+/K^+-ATPase in neurons may contribute to the pathogenesis of diseases such as stroke and dementia (reviewed in [de Lores Arnaiz & Ordieres, 2014]). Taken together, these findings demonstrate that adequate Na^+/K^+-ATPase activity is essential for normal nervous system function.

Our understanding on the specific roles of Na^+/K^+-ATPase subunit isoforms, especially α3, in central nervous system (CNS) function could be significantly improved by knowing the expression patterns of Na^+/K^+-ATPase isoforms in different brain regions and within neuronal populations at the single-cell level. Previous histological studies of α isoform expression in the brain have shown that neurons express multiple α isoforms with variation between different cell types (McGrail et al., 1991). However, isoform expression has not been systematically quantified among individual cells. Therefore, it is still unclear whether all neurons of a particular type (such as interneurons) express the same Na^+/K^+-ATPase isoforms, or if there are subpopulations of neurons and brain regions with differing isoform expression. Related questions are whether neurons co-express multiple Na^+/K^+-ATPase isoforms, as has been shown in cardiac tissue (Harada et al., 2006), and which α-β isoform combinations predominate in each region and neuronal type.

Recent advances in single-cell sequencing technologies have made possible the assessment of the expression level of target genes within thousands of individual cells, enabling the discovery of cellular heterogeneity of gene expression. Two recent studies have provided single-cell transcriptomes for the whole CNS from adult mice (Saunders et al., 2018; Zeisel et al., 2018). In this study, we used these two databases to analyze the expression patterns of all Na^+/K^+-ATPase subunits and their respective isoforms among brain regions and cell types. We identified the populations of neurons in which α3 transcripts are enriched and asked whether expression of other genes could potentially be correlated. We expect that this comprehensive analysis will be a useful source of information to those interested in the pathogenesis of neurological diseases related to the Na^+/K^+-ATPase.

2 | METHODS

2.1 | Dataset preprocessing

The gene raw counts and the cell type annotation for each single cell were downloaded from two online databases published by Dr. McCarroll's lab (http://dropviz.org/, Saunders et al., 2018) and Dr. Linnarsson's lab (http://mousebrain.org/, Zeisel et al., 2018). The raw counts containing the unique molecular identifier (UMI) counts/gene/cell were filtered to discard: (1) cells with robust (>55%) mitochondrial gene expression, (2) cells expressing less than 50 or more than 7500 genes, (3) cells with total read number less than 100 or more than 50,000, and (4) genes that were not expressed or were detected in less than three cells. The intention of this initial filter is to exclude the low-quality cells, which include broken cells which might result in low genes, low UMIs, or robust mitochondrial genes (Ilicic et al., 2016), and doublets that are likely to have extreme high genes or UMIs.

The two filtered gene expression datasets were further processed using the Seurat 3 package (Stuart et al., 2019). Briefly, the two count matrices were normalized using the Seurat "NormalizeData" function with default settings. Batch-effect correction for each dataset was implemented through the Seurat "ScaleData" function using the number of UMI and mitochondrial gene expression detected per cell. The UMAP visualization plots (Figure S1) for the two datasets show that the common cells from different batches were mixed well after adjusting batch effect regardless of whether all cells or only cells from the cerebellum, the brain region we were particularly interested in, were used for plots, indicating the robustness of batch-effect correction. The batch information from database (Saunders et al., 2018) was extracted using the cell ID which was formatted as "batch.ID"_"single.cell.ID," while the batch information from database (Zeisel et al., 2018) was extracted from the column "Flowcell" in their annotation file. The values for gene expression in the finalized datasets were converted from corrected counts to the adjusted $\log_2(\text{CPM} + 1)$, where CPM represents the counts per million reads mapped. For the subsequent analysis, the clustering information for individual cells was inherited from the downloaded cell type annotation files. The mean expression value of a target gene in a cell class or in a neuronal cluster is the arithmetic mean of the gene expression values of individual cells

within that cell class or neuronal cluster. The percentage of positive cells for a target gene in a cell class or in a neuronal cluster is the proportion of cells with non-zero expression of the target gene in that cell class or cluster.

2.2 | Z score for α gross product per cell cluster

To estimate the abundance of α1 or α3 mRNA molecules in each cluster, the gross product of α1 or α3 transcripts is defined as:

$$Prod_i = mean_i * proportion_i$$

where $Prod_i$ is the α1 or α3 product of the cluster i, $mean_i$ is the mean expression value of α1 or α3 transcripts of the cluster i, and $proportion_i$ is the proportion of cells expressing α1 or α3 in the cluster i.

The Z score represents the weight of the α1 or α3 gross product of a specific cluster as compared to the rest of the clusters, described by the equation:

$$Z_i = \frac{Prod_i - \mu}{\sigma}$$

where Z_i is the Z score of the cluster i, $Prod_i$ is the α1 or α3 gross product of the cluster i, μ and σ are the mean and standard deviation of α1 or α3 products of all clusters except the cluster i, respectively.

2.3 | Statistical analysis for co-expression between Na^+/K^+-ATPase subunits and isoforms

Statistical calculations were performed using R (Team, 2019). To evaluate the magnitude of gene co-expression between the different Na^+/K^+-ATPase subunits and isoforms, Spearman's correlation coefficients between all possible subunit and isoform pairs were calculated in all clusters using the mean expressions of isoforms within each cluster. We decided to calculate Spearman's correlation instead of Pearson's correlation for evaluating the gene–gene correlation, due to its outstanding performance at analyzing scRNA-seq libraries (Hou et al., 2019). Although both methods have been utilized to analyze scRNA-seq data, Spearman's correlation is less sensitive to outliers, compared to Pearson's correlation. The R function heatmap.2 was utilized to generate the heatmaps for the visualization of the mean expression values of the Na^+/K^+-ATPase subunits and isoforms.

In its general form, Euclidean distance between two vectors X and Y of n elements is defined as the square root of the sum of squared differences between corresponding elements of the two vectors, shown below:

$$d(x,y) = \sqrt{\sum_i^n (x_i - y_i)^2}$$

For Euclidean distance between two neuronal clusters X and Y containing n genes, x_i and y_i refer to the expression of gene i in each cluster. These distances were used to create the dendrograms shown in the heat maps.

For Euclidean distance between two genes X and Y in n clusters, x_i and y_i refer to the expression of each gene in cluster i. These distances were used to create the dendrograms that represent the relationships of transcript expression similarity among Na^+/K^+-ATPase subunits and neurotransmitter markers.

R function "dist" was implemented to calculate Euclidean distances, which were subsequently examined by Ward's hierarchical agglomerative clustering method using R function "hclust" with Ward's method "ward.D2." Briefly, the pair of neuronal clusters (or genes) with minimum distance the three isoforms tested (or the seven genes tested) was identified and merged, and this agglomeration step was repeated until all neuronal cluster (or genes) were merged, resulting in a hierarchical clustering of n *neuronal clusters* (or genes). For the gene expression dendrogram trees, a similar approach was applied. The distance for merged clusters (or genes) was assessed by the Lance–Williams formula (Szekely & Rizzo, 2005), show below:

$$d(C_i \cup C_j, C_k) = \frac{n_i + n_k}{n_i + n_j + n_k} d(C_i, C_k) + \frac{n_j + n_k}{n_i + n_j + n_k} d(C_j, C_k) - \frac{n_k}{n_i + n_j + n_k} d(C_i, C_j)$$

where C_i, C_j, and C_k refer to three disjoint vectors with sizes n_i, n_j, and n_k respectively.

Eventually, the R function "plot" was used to represent the obtained hierarchical clustering as dendrograms.

2.4 | Correlation analysis to identify relevant genes co-expressed with α isoforms

We performed co-expression analyses for α1 and α3 isoforms using neuronal clusters in which these isoforms are enriched. A series of filters were applied to remove genes with low expression, cells not expressing selected genes and cells expressing a large number of different genes. These filters are necessary because scRNA-seq data have lower sensitivity and higher level of technical noise than bulk RNA-seq data. Thereby, low-expression genes are prompt to introduce bias in correlation analysis. To better describe the context and rationale of these filters, they will be outlined in the Result Section. For those genes and cells remaining after filtering, we calculated the Spearman's correlation coefficients and the false discovery rate (FDR) adjusted p values between for all gene pairs. The FDR-adjusted p values were calculated via Benjamini-Hochberg approach, which is defined as (Benjamini et al., 2009):

$$p_i^{adj} = \min\left\{ \min_{j \geq i} \left\{ \frac{n * p_j}{j} \right\}, 1 \right\}$$

where p_i^{adj} is the adjusted p value, n is the total number of p values, and j is the rank of p_j after ordering all p values from small to large.

2.5 | Gene ontology analysis

Gene ontology enrichment analyses were performed using ShinyGo software package v0.61 (FDR < 0.05) (Ge et al., 2020) and DAVID v6.8 online server (https://david.ncifcrf.gov/tools.jsp) to conduct Gene Ontology (GO) (Huang da, Huang da et al., 2009). Gene symbol lists for the top 100 genes positively correlated with the expression of α1 or α3 isoforms were submitted to search for possible enrichment in biological processes using both packages. In ShinyGo software package v0.61, the strength of a selection is based on the p value, which depends on the number of submitted genes matching a specific biological process and the total number of genes assigned to the process by the database, followed by FDR correction. The software generates hierarchical clustering trees that summarize the significant biological processes, according to their enrichment FDR value. The smaller the value, the more confidence the biological process is represented by the top 100 genes. The analysis using DAVID server was implemented based on the workflow in the user's manuals (https://david.ncifcrf.gov/content.jsp?file=functional_annotation.html), using official gene symbol as the retrieval identifier and *Mus musculus* as the background.

2.6 | Immunostaining for α1 and α3 isoforms

Wild-type mice (2-month-old) were anesthetized with isoflurane and subsequently perfused with 4% paraformaldehyde (PFA). Brain tissues were collected and post-fixed in 4% PFA at 4°C overnight and then cryoprotected with 30% sucrose in phosphate-buffered saline (PBS). Coronal slices of the cerebellum (50 μm) were obtained with a cryostat (Leica CM3050 S, Germany) and processed for immunofluorescence. Antibodies for fluorescence and confocal microscopy were monoclonal antibody to α3 isoform (1:500 dilution; Cat. # ab2826, Abcam) and monoclonal antibody to α1 isoform 1 (1:100 dilution; Cat. # a6F, Developmental Studies Hybridoma Bank).

2.7 | Antibody characterization

The Anti-ATP1A3 antibody (1:500 dilution; Cat. # ab2826, Abcam) was a monoclonal antibody raised against canine cardiac microsomes in the laboratory of Dr. Kevin Campbell (HHMI, University of Iowa) (Arystarkhova & Sweadner, 1996). It stained a pattern of Na^+/K^+-ATPase α3 isoform in mouse interneurons (Picton et al., 2017).

The ATP1A1 antibody (1:100 dilution; Cat. # a6F, Developmental Studies Hybridoma Bank) was a polyclonal antibody raised against purified chicken kidney alpha subunit (Takeyasu et al., 1988). It visualized α1 isoform in the plasma membrane of rat hippocampal neurons (Azarias et al., 2013).

3 | RESULTS

3.1 | Differential expression pattern of Na^+/K^+-ATPase subunits in distinct cell classes

After filtering out low-quality cells (see Methods), 319,320 cells from (Saunders et al., 2018) database and 160,783 cells from (Zeisel et al., 2018) database remained to be used for subsequent analysis. The two raw count matrices from these cells were normalized and scaled using the Seurat package (see Methods). Using the identities of individual cells given in the downloaded cell type annotation files, we annotated 565 and 265 cell clusters from (Saunders et al., 2018) and (Zeisel et al., 2018) databases, respectively. Among these cell clusters, 9 cell classes were identified for the adult mouse nervous system, including CNS neurons, neurogenesis, peripheral nervous system (PNS) neurons, astrocytes, oligodendrocytes, ependymal, peripheral glia, immune, and vascular cells. Expectedly, CNS neurons are the cell class with the largest diversity of unique clusters recognized in both databases (Table S1).

To study the expression profiles of Na^+/K^+-ATPase subunits in different cell classes, we examined the mean expression level of all isoforms of the Na^+/K^+-ATPase subunits as well as the percentage of cells expressing a specific isoform (positive cell) within each cell class. As shown in Figure 1 and Table S2, both databases displayed a comparable expression profile of the different subunit isoforms of the Na^+/K^+-ATPase subunits among those cell classes that were common to the two datasets. Consistent with previous reports, subunit isoforms exhibited distinct cell type-dependent expression patterns. For example, α1 isoform (*Atp1a1*) was ubiquitously detected in both neuronal and non-neuronal cells. Its expression was enriched in CNS neurons, oligodendrocytes, and ependymal cells, but not in astrocytes. α2 isoform (*Atp1a2*) broadly expressed in non-neuronal cells, particularly in astrocytes, while α3 isoform (*Atp1a3*) was neuron-specific, especially in CNS neurons. α4 isoform (*Atp1a4*) was not found in any cell class, which serves as an additional quality control of the data since it is exclusively expressed in testis (McDermott et al., 2012). The β1 isoform (*Atp1b1*) predominated in CNS neurons, while β2 (*Atp1b2*) and β3 (*Atp1b3*) isoforms were found mostly in astrocytes and oligodendrocytes respectively. The expression of small regulatory subunits (*Fxyds*) also varied largely among different cell classes. *Fxyd1* isoform was mainly found in glial cells, while *Fxyd6* and *Fxyd7* isoforms were present in CNS and PNS neurons, yet the latter also expressed *Fxyd2* isoform. *Fxyd5* isoform was found in vascular cells of the brain.

3.2 | Transcriptional profile of Na^+/K^+-ATPase isoforms in CNS neurons

CNS neurons, as the largest cell population in the mouse nervous system, were annotated into 324 and 160 clusters in (Saunders et al., 2018) and (Zeisel et al., 2018) databases, respectively. In each neuronal CNS cluster, we calculated and compared the mean expression of the relevant Na^+/K^+-ATPase isoforms. Figure 2a1,a2 show

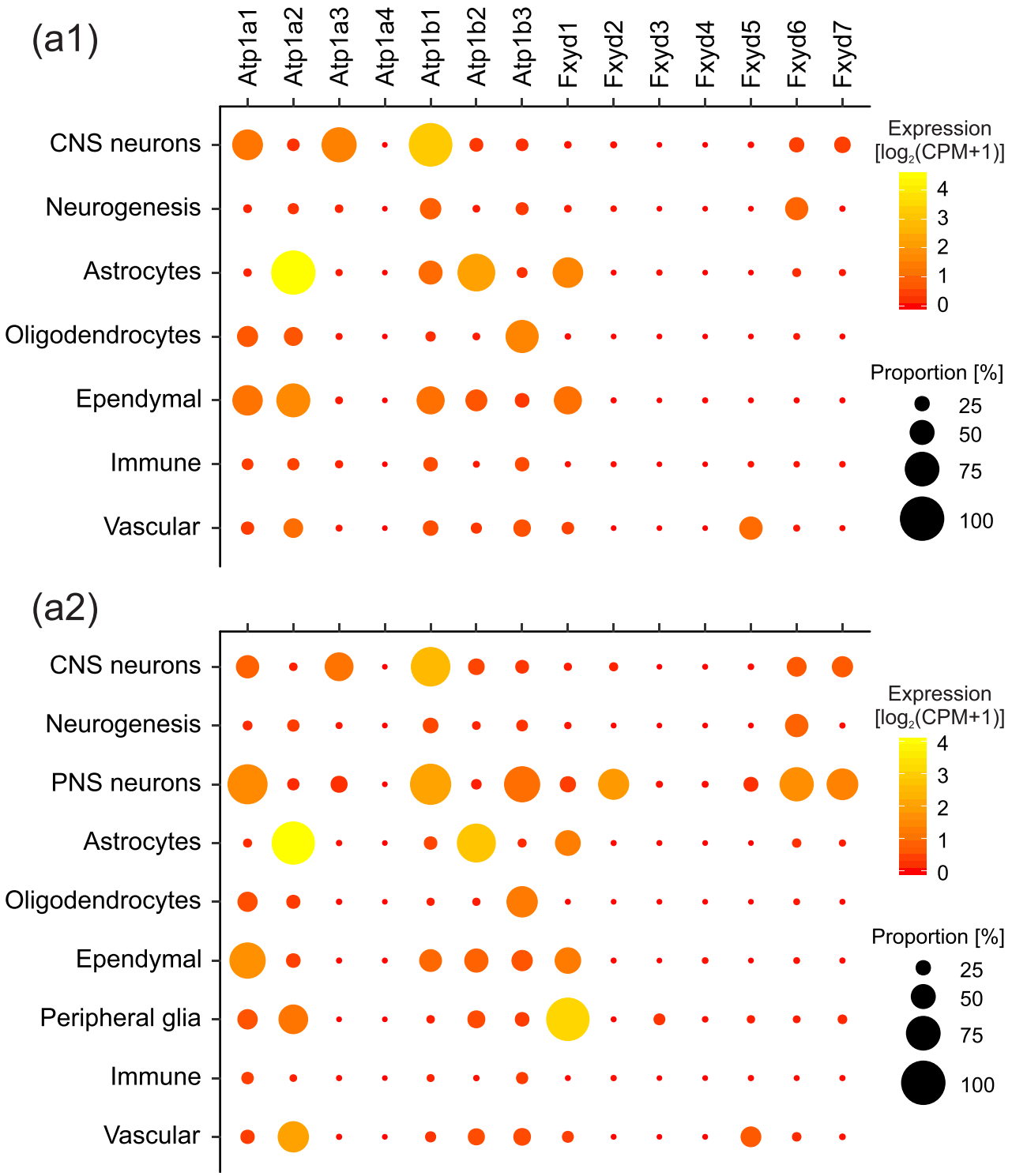

FIGURE 1 Expression and proportion of transcripts encoding the Na^+/K^+-ATPase subunits and isoforms in various cell classes. Each circle represents one Na^+/K^+-ATPase isoform in a specific cell class. The color and size of each circle represent the average expression level and the proportion of cells expressing the corresponding isoform, respectively. (a1) and (a2) were generated using data from Saunders et al. (2018) and Zeisel et al. (2018) databases, respectively. The determinations of expression and proportion are described in Section 2.1

that in both datasets α1, α3, β1, *Fxyd6*, and *Fxyd7* were the major Na^+/K^+-ATPase isoforms in mouse CNS neurons, yet there are variations of expression levels among isoforms. Given that the core enzyme consists of a heterodimer of one α and one β subunit, these results indicate that most of the functional Na^+/K^+-ATPases in CNS neurons contain α1/β1 and α3/β1 complexes. Indeed, in CNS neurons expressing α1 or α3, β1 transcripts are predominant (Fig. 2a1, a2, Figure S2). Further, in all cases in which β1 transcripts co-expressed with either β2, β3, or both, the expression values for β1 transcripts were always higher (Table S3).

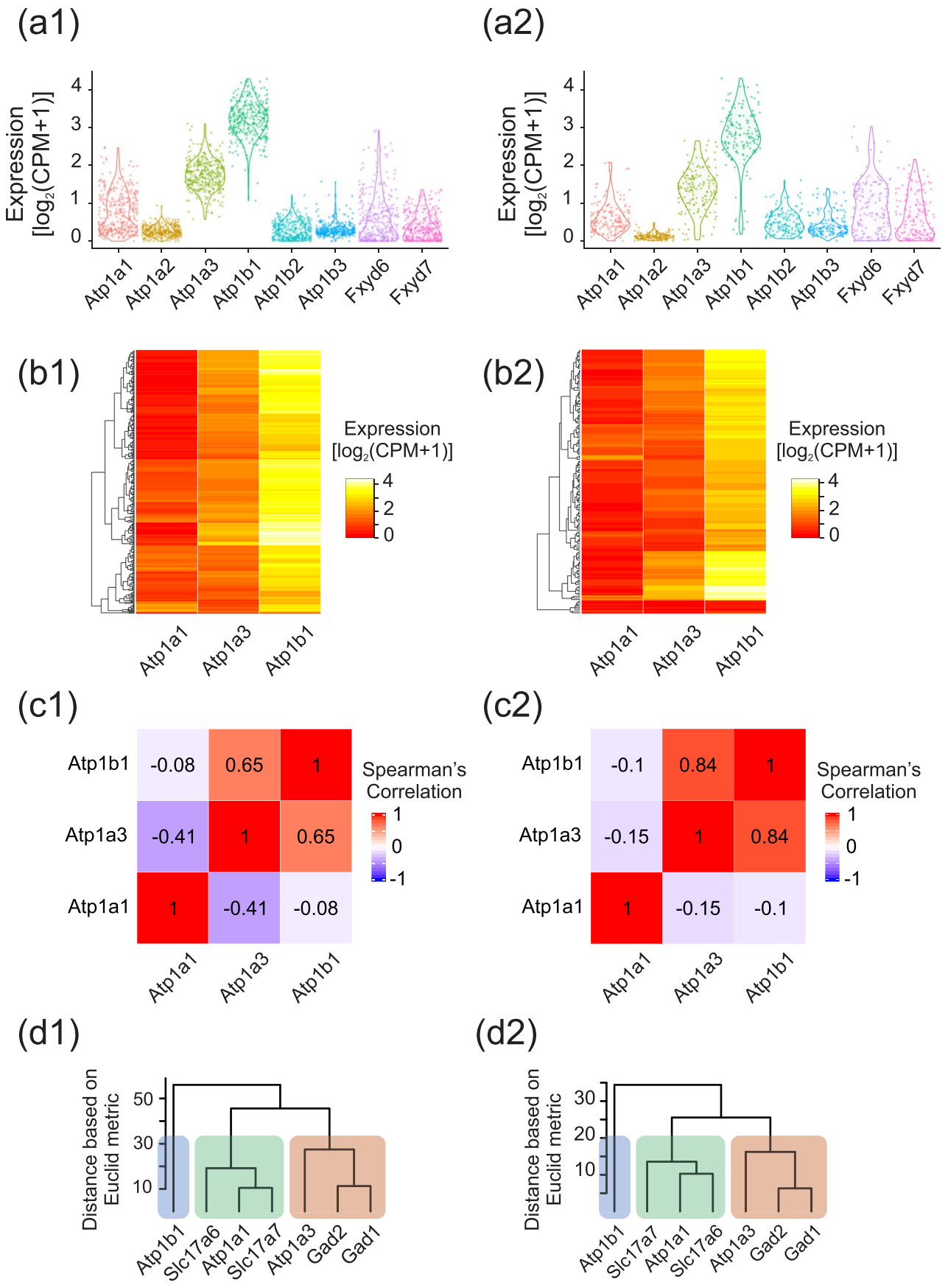

FIGURE 2 Legend on next page.

Next, we asked whether expression of subunits in functional Na^+/K^+-ATPase complexes are correlated at the transcript level. Figure 2b1,b2 show hierarchical clustering heatmaps for α1, α3, and β1 from both datasets. β1 isoform is ubiquitously present in most neuronal populations, while α1 and α3 transcripts appear to be sometimes negatively correlated with each other. Quantitively, these co-expression patterns of α1, α3, and β1 isoforms were further confirmed by estimating the Spearman's correlation between these three isoforms in CNS neurons (Figure 2c1,c2). Figure S3 shows these plots for the major Na^+/K^+-ATPase isoforms present in CNS neurons.

Are inhibitory or excitatory neurons poised to preferentially express α1 or α3 isoforms? To address this question, we computed, for both datasets, pairwise Euclidean distances among α1, α3, and β1 isoforms of the Na^+/K^+-ATPase, together with two marker genes for excitatory neurons (*Slc17a6* and *Slc17a7*) and two marker genes for inhibitory neurons (*Gad1* and *Gad2*). The complete list of expression values for these target genes among all neuronal clusters from both datasets is available as Table S4. Based on the divergence in gene expression patterns in all CNS neuronal clusters, in both datasets, the Euclidean distance calculations and hierarchical agglomeration (see Methods) classified three groups: *Atp1b1*, *Atp1a1* together with the two excitatory marker genes and *Atp1a3* together with the two inhibitory marker genes (Figure 2d1,d2). These results suggest that there is a tendency for clusters expressing predominantly α1 isoform to be associated with excitatory neurotransmitter markers, while those clusters predominantly expressing α3 isoform do so with inhibitory neurotransmitters. It is important to consider that the observed association is not exclusive. Individual clusters can express either or both isoforms, and some neurons that predominantly express α3 isoforms are excitatory and vice versa. The tendency and examples of non-exclusivity can be found in Tables 1–4. These results confirm previous findings at the RNA and protein level that the α3 subunit is predominantly expressed in

TABLE 1 Transcript expressions for the Na^+/K^+-ATPase isoforms and neurotransmitter markers in neuronal clusters with Z scores larger than 2 for *a1* isoform from (Saunders et al., 2018) database

Cluster name	Atp1a1	Atp1a3	Slc17a6	Slc17a7	Gad1	Gad2	Region	Cluster common name
FC_6-6	2.538	2.105	0.000	2.056	0.000	0.836	Frontal cortex	Deep layer pyramidal cells
PC_2-1	2.546	0.955	0.413	1.276	0.020	0.029	Posterior cortex	Neurofilament, Layer4?
PC_2-10	2.294	1.134	0.624	1.196	0.018	0.026	Posterior cortex	Layer 5a
PC_2-7	2.257	1.413	0.187	1.622	0.021	0.028	Posterior cortex	Layer 2/3
FC_6-1	2.212	1.105	0.062	1.471	0.012	0.022	Frontal cortex	Superficial layer pyramidal cells—Layer 2/3
PC_2-5	2.171	1.101	0.255	1.359	0.017	0.024	Posterior cortex	Layer 2/3
FC_6-3	2.132	1.167	0.228	1.605	0.011	0.020	Frontal cortex	Deep layer pyramidal cells—Layer 5a
PC_2-4	2.064	1.032	0.175	1.459	0.012	0.014	Posterior cortex	Layer 2/3, IEG+
PC_2-11	2.050	1.207	0.341	1.305	0.013	0.024	Posterior cortex	Layer 5a
PC_3-1	1.957	1.681	0.121	1.191	0.008	0.018	Posterior cortex	Layer 5a, entorhinal cortex, Cbln1+
PC_2-2	2.031	1.277	0.224	1.239	0.024	0.030	Posterior cortex	Retrosplenial cortex (RSG)/Entorhinal cortex, Layer 2/3
PC_2-9	1.861	1.336	0.107	1.464	0.017	0.030	Posterior cortex	Layer 5a, BC006965+
HC_3-4	1.676	1.876	0.298	1.144	0.112	0.000	Hippocampus	Entorhinal cortex
PC_2-14	1.790	1.335	0.519	1.238	0.020	0.029	Posterior cortex	Retrosplenial cortex (RSG)/Subiculum/Parasubiculum

Note: Expression values represent the average value of the expression of the gene in that cluster, of which brain region and common name are also provided. All values were rounded to 3 decimal places. The cluster names, regions and their common names were inherited from the downloaded cell type annotation files of the published online scRNA dataset.

FIGURE 2 Expression and correlation of Na^+/K^+-ATPase subunits and their isoforms within the CNS neuronal clusters. (a1,a2) Violin plots for mean expressions of Na^+/K^+-ATPase subunits and isoforms within CNS neuronal clusters. Each dot represents one neuronal cluster, while each violin plot reflects the expression distribution of each individual isoform in the neurons from the mouse brain. (b1,b2) Heatmaps of mean expressions for α1, α3, and β1, the major candidates to form the minimal functional Na^+/K^+-ATPase complexes. Each row represents one neuronal cluster, while the color is assigned according to the mean expression value of the gene in the corresponding cluster. More comprehensive heatmaps of all CNS Na^+/K^+-ATPase subunits and isoforms are shown in Figure S3. (c1,c2) Spearman's correlation coefficients between α1, α3, and β1. The colors are assigned according to the values of correlation coefficients. Spearman's correlation coefficients between all CNS Na^+/K^+-ATPase subunits and isoforms are shown in Figure S3. (d1,d2) Euclidean distance trees for the α1, α3, β1, and neurotransmitter markers. The distance refers to the divergence between gene expression profiles. The colors represent the grouping of genes based on the pairwise distances. a1, b1, c1, and d1 were generated using data from Saunders et al. (2018), while a2, b2, c3, and d3 were made using data from Zeisel et al. (2018). The average gene expression per cluster was determined as described in Section 2.1. Spearman's correlations in (b,c) and Euclidean distances in Figure 2(d) were calculated as described in Section 2.3

TABLE 2 Transcript expressions for the Na^+/K^+-ATPase isoforms and neurotransmitter markers in neuronal clusters with Z scores larger than 2 for *a1* isoform from (Zeisel et al., 2018) database

Cluster name	Atp1a1	Atp1a3	Slc17a6	Slc17a7	Gad1	Gad2	Region	Cluster common name
TEGLU7	2.069	0.740	0.067	2.001	0.045	0.019	Cortex	Excitatory neurons, cerebral cortex
TEGLU8	2.053	0.727	0.112	2.164	0.031	0.011	Cortex	Excitatory neurons, cerebral cortex
TEGLU9	1.912	1.017	0.096	2.371	0.016	0.027	Cortex	Excitatory neurons, cerebral cortex
TEGLU4	1.896	1.834	0.089	2.620	0.037	0.013	Cortex	Excitatory neurons, cerebral cortex
CBINH2	1.861	2.387	0.000	0.120	1.858	1.307	Cerebellum	Granular layer interneurons, cerebellum
TEGLU16	1.509	1.106	0.165	2.371	0.036	0.030	Cortex	Excitatory neurons, cerebral cortex
TEGLU10	1.499	1.307	0.058	3.138	0.019	0.020	Cortex	Excitatory neurons, cerebral cortex
TEGLU11	1.405	1.155	0.006	2.789	0.037	0.016	Cortex	Excitatory neurons, cerebral cortex
HBINH8	1.207	2.491	0.000	0.000	3.609	1.693	Medulla	Inhibitory neurons, hindbrain

Note: Expression values represent the average value of the expression of the gene in that cluster, of which brain region and common name are also provided. All values were rounded to 3 decimal places. The cluster names, regions and their common names were inherited from the downloaded cell type annotation files of the published online scRNA dataset.

TABLE 3 Transcript expressions for the Na^+/K^+-ATPase isoforms and neurotransmitter markers in neuronal clusters with Z scores larger than 2 for *a3* isoform from (Saunders et al., 2018) database

Cluster name	Atp1a1	Atp1a3	Slc17a6	Slc17a7	Gad1	Gad2	Region	Cluster common name
CB_4-2	0.611	3.189	0.000	0.054	2.885	3.072	Cerebellum	Golgi interneuron
CB_3-2	0.729	3.114	0.000	0.029	3.004	2.234	Cerebellum	Cerebellum basket cells 2
CB_3-1	0.459	3.018	0.000	0.006	2.006	1.905	Cerebellum	Cerebellum basket cells 1
CB_3-3	0.393	2.943	0.000	0.000	2.148	2.479	Cerebellum	Cerebellum basket cells 3
STR_14-1	0.190	2.674	0.000	0.000	3.343	3.026	Striatum	Fast-spiking interneuron, Pvalb+
HC_1-25	0.437	2.638	0.000	0.081	2.374	3.774	Hippocampus	Interneuron, (candidate CGE-derived 10)
HC_5-13	0.413	2.588	0.482	0.814	0.032	0.000	Hippocampus	Postsubiculum
STR_14-3	0.286	2.630	0.000	0.000	3.234	3.160	Striatum	Fast-spiking interneuron, Pvalb+/Rgs12+
CB_4-1	0.151	2.620	0.524	1.015	0.000	0.000	Cerebellum	Unipolar brush cell
HC_1-6	0.293	2.649	0.011	0.051	2.923	2.500	Hippocampus	Interneuron, Basket 1
HC_1-7	0.120	2.574	0.006	0.077	2.552	1.835	Hippocampus	Interneuron, Basket 1
HC_1-10	1.011	2.635	0.000	0.094	2.705	2.849	Hippocampus	Interneuron, OLM4 (Dentate enriched?)

Note: Expression values represent the average value of the expression of the gene in that cluster, of which brain region and common name are also provided. All values were rounded to 3 decimal places. The cluster names, regions and their common names were inherited from the downloaded cell type annotation files of the published online scRNA dataset.

TABLE 4 Transcript expressions for the Na^+/K^+-ATPase isoforms and neurotransmitter markers in neuronal clusters with Z scores larger than 2 for *a3* isoform from (Zeisel et al., 2018) database

Cluster name	Atp1a1	Atp1a3	Slc17a6	Slc17a7	Gad1	Gad2	Region	Cluster common name
HBGLU7	0.379	2.644	1.575	2.580	0.008	0.070	Pons	Excitatory neurons, hindbrain
HBGLU8	0.503	2.610	2.026	2.760	0.000	0.086	Pons	Excitatory neurons, hindbrain
HBINH7	0.246	2.644	0.000	0.000	1.396	0.994	Pons	Inhibitory neurons, hindbrain
HBGLU9	0.160	2.531	2.207	0.956	0.000	0.032	Medulla	Excitatory neurons, hindbrain
HBINH8	1.207	2.491	0.000	0.000	3.609	1.693	Medulla	Inhibitory neurons, hindbrain
HBGLU6	0.355	2.417	1.663	2.446	0.005	0.328	Pons	Excitatory neurons, hindbrain

Note: Expression values represent the average value of the expression of the gene in that cluster, of which brain region and common name are also provided. All values were rounded to 3 decimal places. The cluster names, regions and their common names were inherited from the downloaded cell type annotation files of the published online scRNA dataset.

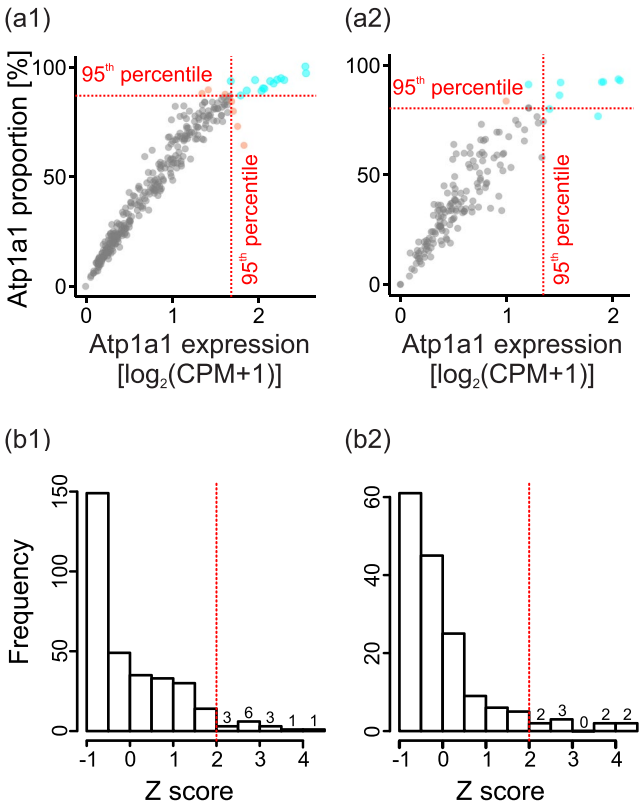

FIGURE 3 Identifying neuronal clusters with high expression of transcripts encoding for α1. (a1,a2) Scatter plots of the expression of α1 transcripts versus the proportion of cells expressing α1 for CNS neuronal clusters. Each circle represents one neuronal cluster. Clusters above the 95th percentile for either variable are shown in coral or cyan, the latter corresponding to those clusters with Z scores higher than 2. Red dotted lines define the 95th percentile limits. (b1,b2) Histograms for Z scores from CNS neuronal clusters. Red dotted lines define Z scores equal to 2. The number of clusters in bins with Z larger than 2 are shown above the bars. a1 & b1 and a2 & b2 were generated using data from Saunders et al. (2018) and Zeisel et al. (2018), respectively. The determinations of expression and proportion were described in Section 2.1. The gross product and Z score were calculated as described in Section 2.2

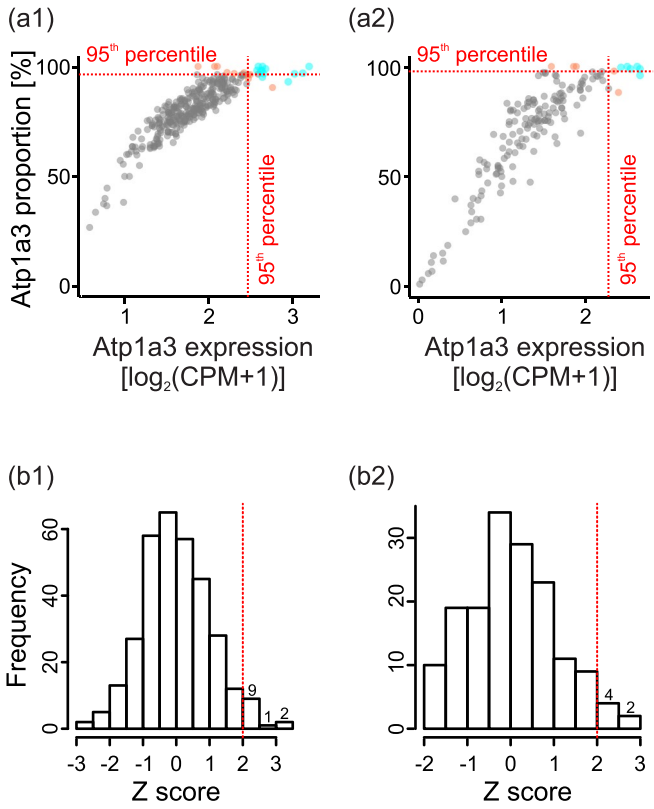

FIGURE 4 Identifying neuronal clusters with high expression of transcripts encoding for α3. (a1,a2) Scatter plots of the expression of α3 transcripts versus the proportion of cells expressing α3 for CNS neuronal clusters. Each circle represents one neuronal cluster. Clusters above the 95th percentile for either variable are shown in coral or cyan, the latter corresponding to those clusters with Z scores higher than 2. Red dotted lines define the 95th percentile limits. (b1,b2) Histograms for Z scores from CNS neuronal clusters. Red dotted lines define Z scores equal to 2. The number of clusters in bins in which Z was >2 are shown above the bars. a1 and b1, and a2 and b2 were generated using data from Saunders et al. (2018) and Zeisel et al. (2018), respectively. The determinations of expression and proportion were described in Section 2.1. The gross product and Z score were calculated as described in Section 2.2

inhibitory neurons in various regions of rodent brains, such as the hippocampus (Bottger et al., 2011; Ikeda et al., 2013; Murata et al., 2020).

Interestingly, at the transcript level we observed that in CNS neurons the expression value of the β subunit tended to be about 50% higher than the expression value of the α subunit (Table S4, statistics spreadsheets). Given that the main function of the β subunit is to assist the assembly and traffic of Na^+/K^+-ATPase complexes, the excess of β subunit transcripts may ensure sufficient trafficking of pumps to the plasma membrane.

3.3 | Identification of neuronal clusters expressing the highest levels of α1 or α3 transcripts in the CNS

To identify those neuronal clusters with the highest expression of transcripts for the α1 or α3 isoforms in the mouse CNS, we applied two criteria in each dataset. First, we plotted the average expression level versus the proportion of cells expressing α1 or α3 isoforms of all CNS clusters for both datasets and implemented 95th percentile filters for both variables. Figures 3a1,a2 and 4a1,a2 show these plots for α1 and α3, respectively. The information of those clusters above at least one of the imposed thresholds are shown as highlighted clusters in Table 5 (α1) and Table 6 (α3). Second, we calculated the Z scores of each cluster from both datasets, plotted their distributions and established a limit at >2, where the Z score represents the distance between the gene gross product (expression mean x proportion) in a specific cluster and the cluster population mean (see Methods). Figures 3b1,b2 and 4b1,b2 show these distributions of Z scores for the isoforms α1 and α3, respectively. The information of those clusters with Z scores larger than 2 are denoted by red fonts in Table S5 (α1) and Table S6 (α3). In both databases, the Z score distributions for the α1 or α3 isoform are

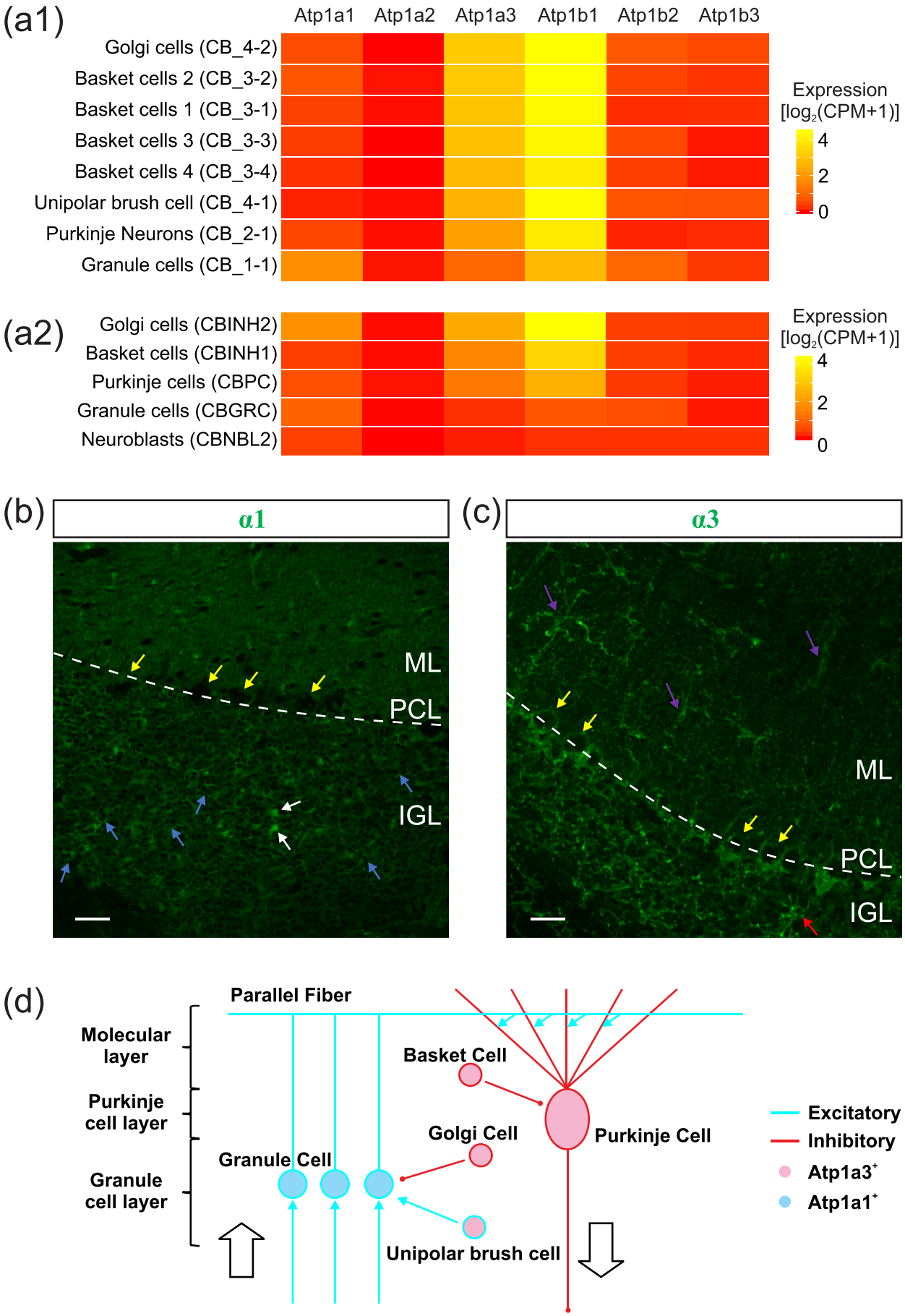

FIGURE 5 Legend on next page.

different. In the case of α3, it appears as a normal distribution, whereas in the case of α1 it does not. The shape of the Z-score distribution inherits the shape of the gross product because the Z score is a linear transformation of the gross product (see Methods). In the case of α1 the distribution of values of expression is skewed towards the low end, while for the α3 isoform the distribution is bell shaped (data not shown). This signifies that α1 transcripts, as a population across all clusters, were less abundant than α3 transcripts.

Clusters that were above the 95th percentile of average expression or positive cell percentage are shown in Figures 3a1,a2 and 4a1, a2 as either coral or cyan circles, the latter representing clusters with a Z score higher than 2. As expected, all cyan clusters meet at least one of the 95th percentile thresholds. Tables 1 and 2 show the annotated names for those neuronal clusters with Z scores for α1 isoform larger than 2 from each database. These tables contain the expression values for the α1 isoform, and, as well, the expression values for the other α isoform (α3, in this case) and the four neurotransmitter markers. The corresponding Tables 3 and 4 contain the same information for those neuronal clusters with Z scores for α3 isoform larger than 2 from each database. Both datasets consistently show that most of the clusters highly expressing α1 isoform (Tables 1 and 2) originate from the Cortex. With two exceptions in Table 2, most of the clusters dominantly express genes associated with excitatory neurotransmission, particularly *Slc17a7*. The two exceptions are the results of our selection method, that is, we only considered the expression values of α1 isoform, yet these two clusters also abundantly expressed α3 isoform and the inhibitory neurotransmitter markers. For the α3 isoform (Tables 3 and 4), in one dataset 10 out of 12 clusters correspond to cell types from the cerebellum or hippocampus, while in the other dataset the six clusters are cell types from the pons and medulla in the hindbrain, also referred to as the brainstem. The potential reason for the discordance between the brain regions in Tables 3 and 4 is that Saunders et al. (Saunders et al., 2018) did not take tissue samples from the pons and medulla, as well as the olfactory bulb. Then, we asked whether removing the clusters which originated from the pons, the medulla and the olfactory bulb in the database of Zeisel et al. (2018) could establish some agreement between the two datasets. Indeed, Figure S4 and Table S7 show nine clusters that meet at least one of the 95th percentile thresholds, of which six are from the hippocampus, the cortex, and the cerebellum. These data combined suggest that the brain regions in mice with highest expression of α3 isoform transcripts are the pons, the medulla, the cerebellum, and the hippocampus. Interestingly, these α3-enriched brain regions have been reported to be related to neurological diseases linked with α3 mutations (Oblak et al., 2014; Saito et al., 1998; Sasaki et al., 2017).

3.4 | Populations of neurons expressing transcripts from the α1 and α3 isoform genes in the context of a neuronal circuit: The cerebellum

To better understand the significance of the distinct expression levels of the neuronal α3 and α1 isoform in the mouse brain, it is useful to characterize the pattern among different neuron subtypes in the context of the circuitry of specific brain regions. We chose the cerebellum because it has a relatively simple neuronal circuitry as compared to the hindbrain or the hippocampus, and it is a region that has been linked to multiple symptoms of AHC.

For this purpose, we first generated two heatmaps, one for each database (Saunders et al., 2018; Zeisel et al., 2018), using the mean expression values for the different α and β isoforms of clusters originated from the cerebellum (Figure 5a1,a2). From these databases, 9 and 5 neuronal clusters were annotated as neuron types coming from the cerebellum by Saunders et al. (Saunders et al., 2018) and Zeisel et al. (Zeisel et al., 2018), respectively. Based on the gene expression signature for cerebellar neurons, these 14 clusters were categorized into seven major populations: Golgi cells, basket cells, Purkinje cells, unipolar brush cells, inferior colliculus, granule cells, and neuroblasts (Figure 5a1,a2). It is worth noting the consistency between both databases. In both, Golgi, basket and Purkinje cells predominantly express the neuronal-specific α3 isoform transcript, while granule cells appear to express more transcripts from the α1 isoform. Consistent with the overall observations of CNS clusters, β1 isoform is the most abundant transcript among Na^+/K^+-ATPase isoforms in the cerebellum. In the cerebellum, the unipolar brush cell cluster is an exception to the general association between neuron's neurotransmission type and abundance of a specific α isoform. The neurons from this cluster are excitatory neurons, yet transcripts from the α3 isoform are predominant.

Overall, the pattern of expression of transcripts for the α1 and α3 isoforms observed in the cerebellum in the two databases is in good agreement with previous histological studies (Bottger et al., 2011; Hieber et al., 1991; Ikeda et al., 2013; McGrail et al., 1991; Peng et al., 1997; Watts et al., 1991). To further support these studies, we

FIGURE 5 Expression spectrum of the α and β isoforms in the mouse cerebellum. (a1,a2) Heatmaps of mean expressions for the α and β isoforms in cerebellar neuronal clusters. Each row refers to each cerebellar neuronal cluster, where its color is assigned according to its expression value. a1 and a2 were generated using data from Saunders et al. (2018) and Zeisel et al. (2018), respectively. The determinations of expression were described in Section 2.1. (b, c) Representative images of immunostaining of mouse cerebellar slices using α1 and α3 antibodies. Purkinje cells (yellow arrow), granule cells (blue arrow), Golgi cells (red arrow), basket cells (purple arrow) and glomeruli (white arrow). GL, granular layer; ML, molecular layer; PCL, Purkinje cell layer. Dashed lines represent the approximate locations of the PCL. $N = 2$ (animals), $n = 8$ (slices) for two-month-old WT mice. Scale = 20 μm. (d) Illustration of the cerebellar neuronal network. Filled-colors refer to the preferential expressions of either α1 (light blue) or α3 (coral), while outline-colors represent whether the neuron is excitatory (cyan) or inhibitory (red)

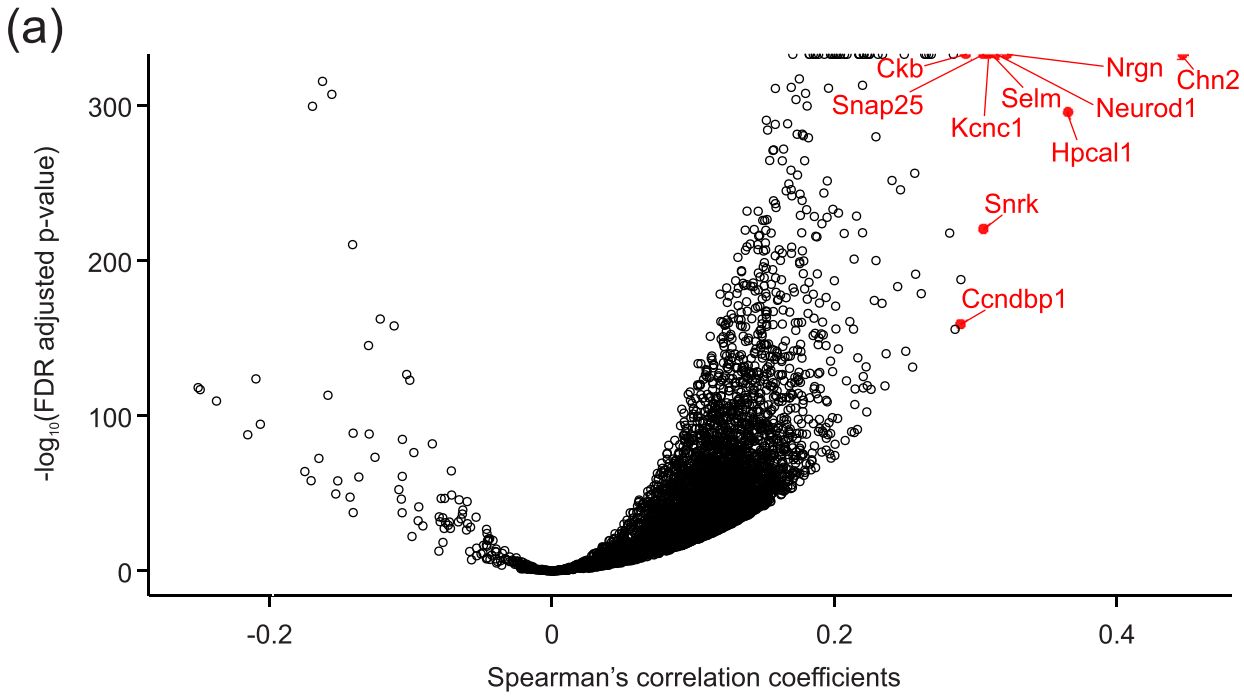

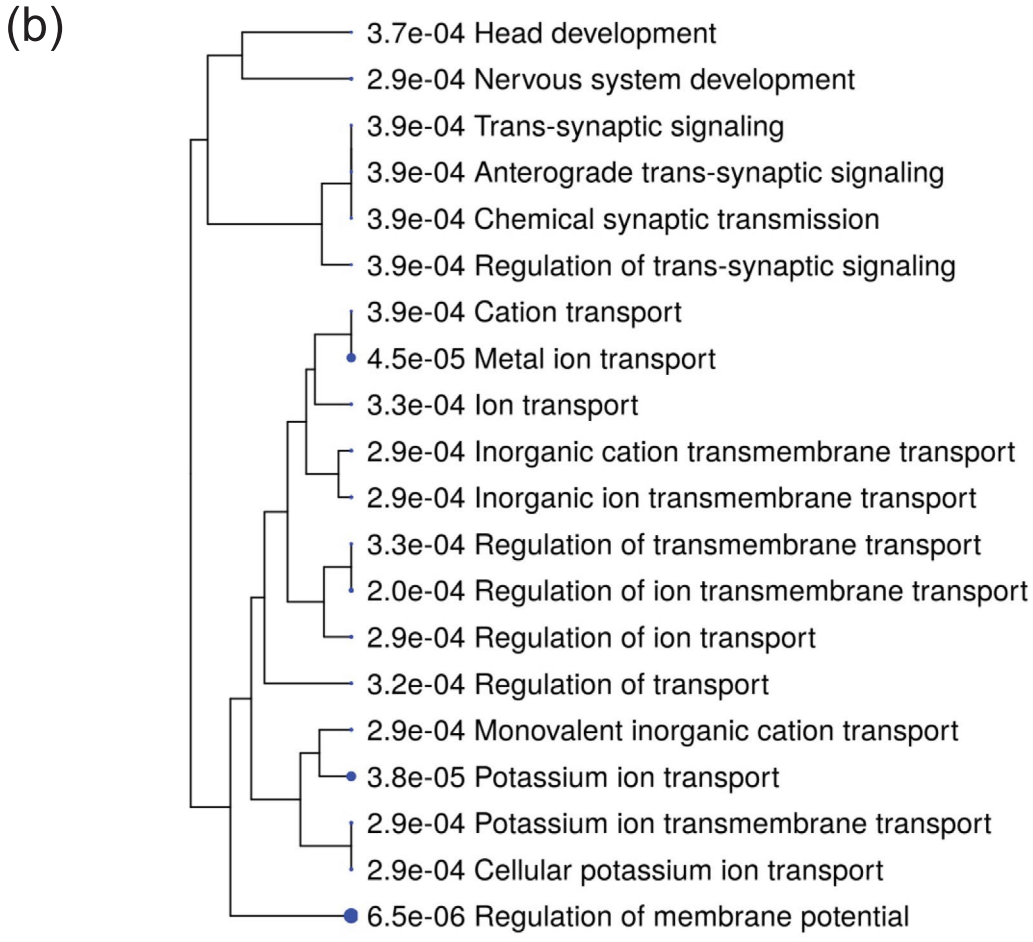

FIGURE 6 Legend on next page.

performed immunohistochemistry assays on adult mouse cerebellar slices (Figure 5b,c). We used the morphology and spatial location to identify the cell types. Experiments using α1 antibodies (e.g., Figure 5b) showed that the soma of Purkinje cells lack α1 subunits (Figure 5b, dark regions in the Purkinje cell layer [PCL], yellow arrows). Clearly, in the granular layer (GL), there are cells abundantly expressing the α1 subunit. There are α1 ring-stained cells which are small (∼5 μm in diameter), numerous, and tightly packed together (Figure 5b, blue arrows), indicating that they are likely granule cells. There are also regions in the GL which are densely labeled and normally adjacent to a granule cell (Figure 5b, white arrows). These regions might represent abundant α1 staining in the complex glomeruli structures. There is more diffuse α1 staining in the molecular layer (ML) (Figure 5b), which likely corresponds to the presence of the α1 subunit in axons from the granule cells. The α3 staining pattern in the cerebellum is notably different than that of α1 staining (Figure 5c). Purkinje cells are now encircled by fluorescence (Figure 5c, yellow arrows), confirming that the α3 subunit is the predominant α isoform in these cells. The GL appears to have substantial α3 staining with a characteristic punctuated pattern. Golgi cells are expected to be in this layer, yet in rodents there is one Golgi cell for every ∼400 granule cells (Korbo et al., 1993), so it would be difficult to detect a Golgi cell among the broad punctuated pattern of the α3 staining. Nonetheless, the size and wide arborization of some cells, such as the one indicated by the red arrow (Figure 5c), were suggestive of Golgi cells. Even though unipolar brush cells are more abundant than Golgi cells and have a characteristic morphology, we cannot establish with confidence that they can be identified by α3 staining. In the ML, there are two main types of interneurons, the stellate cells, and the basket cells. The latter type was the only one identified in both databases. The basket cells are mainly located in the lower half of the ML, like the cells indicated by purple arrows (Figure 5c). Overall, these results are consistent with our statistical analysis of the two databases, as well as previous studies at the protein and mRNA level (Bottger et al., 2011; Hieber et al., 1991; Ikeda et al., 2013; McGrail et al., 1991; Peng et al., 1997; Watts et al., 1991).

Combining the information at the mRNA and protein levels described above, Figure 5d shows a simple anatomical illustration of the cerebellar neuronal circuitry, in the context of the predominant α isoform in each type of neuron. Clearly, the processing of electrical activity in the cerebellum is determined by neurons that predominantly express the α3 isoform. Therefore, it is not surprising that this brain region is implicated in disorders linked to mutations of this isoform. In summary, our analysis and data strengthen the importance of the α3 isoform in the local cerebellar network.

3.5 | Correlation analysis to identify relevant genes that co-express with α1 and α3 isoforms

We next asked whether the expression of transcripts from the α1 and α3 isoforms correlated to the expression of transcripts from other genes, which would provide a more systematic perspective of their function and identify genes involved in common biological processes.

To identify the co-expression networks for α1 and α3 isoforms, we considered only the top α enriched neuronal clusters identified by percentile thresholding (Figures 3a1,a2 and 4a1,a2). For each α isoform, we combined the clusters from both databases, totaling 31 clusters for the α1 isoform and 34 clusters for the α3 isoform. We first examined the expression spectrum of all detected genes across the selected neuronal clusters and noticed a large proportion of genes with low expression, as is commonly observed in most scRNA-Seq studies. The quantification of low-expressed genes could be less reliable and may hinder downstream correlation analysis. Therefore, we implemented an expression threshold (referred as *Expr25*), to discard those genes with average values of expression lower than the 25th percentile of all the mean expression values. The filtered subdataset for α1 enriched clusters was composed of 20,515 genes and 66,328 cells, while the filtered subdataset for α3 enriched populations was composed of 15,962 genes and 3930 cells. The large difference between the number of cells in these two subdatasets is due to the overwhelming number of granule cells sequenced. As expected, *Atp1a1* and *Atp1a3* remained in both filtered subdatasets.

Then, we generated submatrices composed by the expression values for either α1 or α3 and the expression values of a test gene in all cells, which are referred as the gene–gene matrices. These matrices contained 2 genes × 66,328 cells and 2 genes × 3930 cells for α1 and α3, respectively (Figure S5). We noticed that in many cells, the value for the expression of a test gene was lower than the 25th percentile established previously. This is likely due to both biological variability and technical difficulties. Even though imputation and data-smoothing could address this issue, these data are prompt to generate false positive gene–gene correlations later. Therefore, we opted for a second filter to discard all cells in a gene–gene matrix that contained expression values less than the expression threshold *Expr25*, established above (Figure S5). Finally, any gene–gene matrix containing less than three cells were also discarded (Decision step "$x \geq 3$" in Figure S5). Only one gene–gene matrix from the α1 was discarded but none for α3. From the filtered gene–gene matrices, we computed three variables: the numbers of cells remaining, the Spearman's correlation coefficients and the corresponding *p* values. The first two variables were visualized in two ways. First, Figure S6a,c show the

FIGURE 6 Genes correlated with the expression of α1. (a) Volcano plot of Spearman's correlation coefficients versus -log10 (FDR-adjusted *p* values). Each symbol represents one test gene. The half-symbols on the top edge is the default manner that R package uses to plot those genes with infinity values. Top 10 genes with highest positive correlations are marked with red color. Spearman's correlation and the corresponding log10 transformed FDR-adjusted *p* values were described in Sections 2.4 and 3.5. (b) A hierarchical clustering tree that summarizes the significant biological processes. The sizes of the blue dots and their corresponding values refer to the Enrichment FDR for the specific biological process, calculated by ShinyGo software (see Section 2.5)

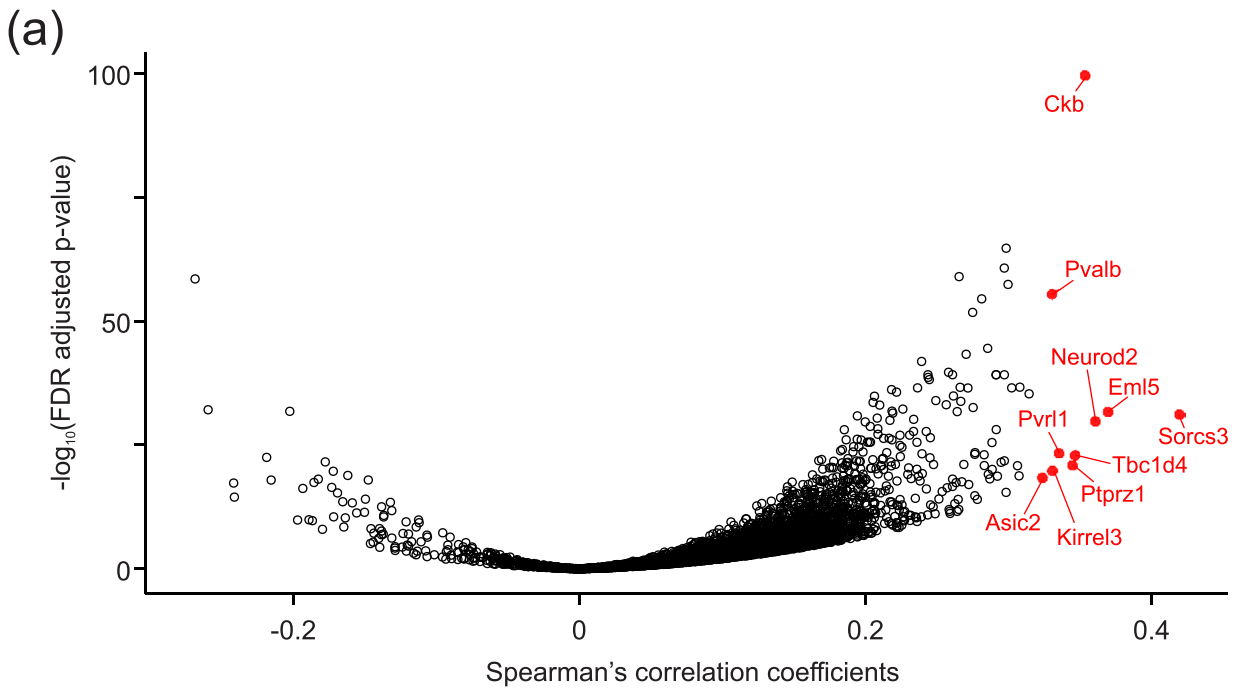

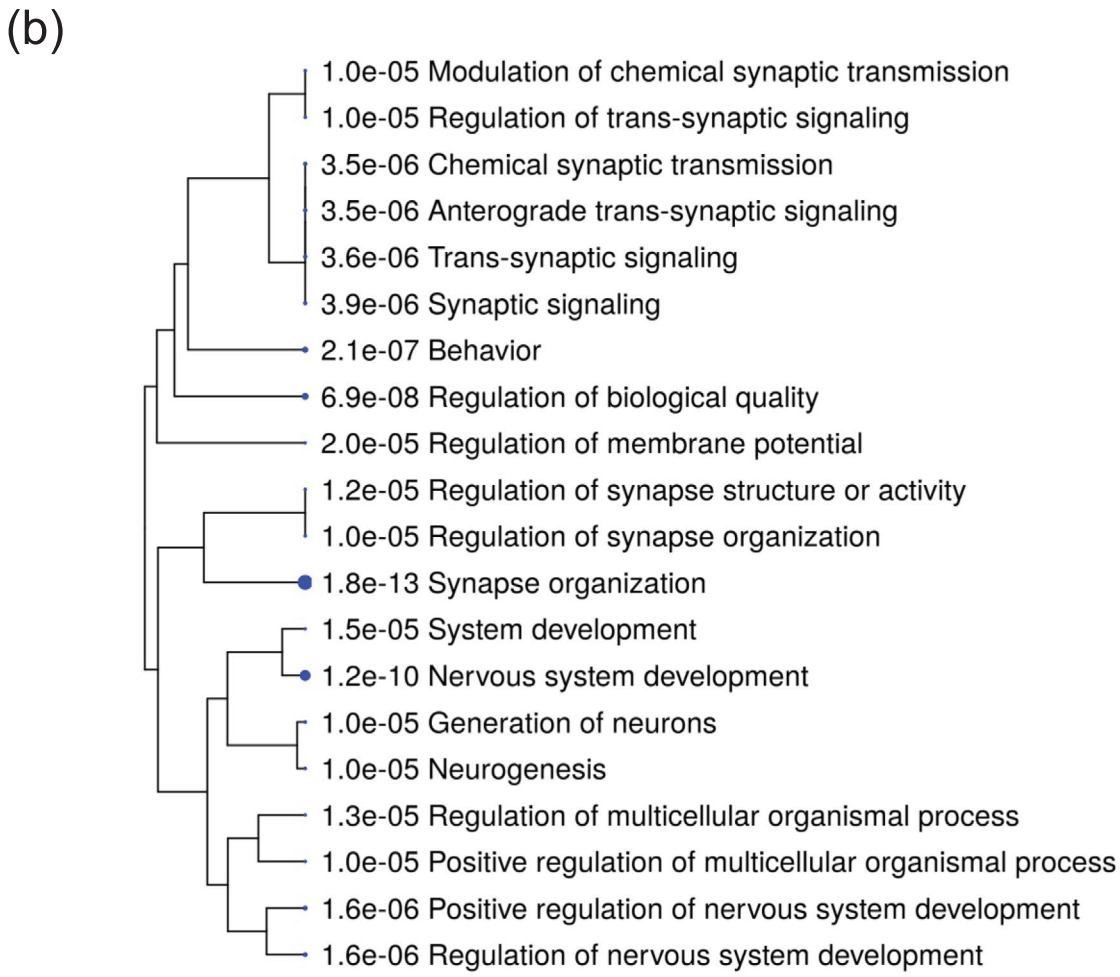

FIGURE 7 Legend on next page.

distributions of the number of cells remaining for α1 and α3, respectively. Both distributions are skewed towards the left, that is, gene–gene matrices containing few cells remaining were dominant. Second, by plotting the number of cells remaining versus the calculated gene–gene Spearman correlation coefficient of all gene–gene matrices (Figure S6b,d), we noticed that these gene–gene matrices with few cells remaining are poised to have high Spearman correlation coefficients. These observations indicate these gene–gene matrices with few cells remaining might introduce additional bias. To reduce this bias, we implemented a stringent threshold at 75th percentile of the distributions of the number of cells remaining, which was referred as the threshold *Num75* (*Num75* = 8275.5 for α1 enriched clusters; *Num75* = 737 for α3 enriched clusters) (Figure S6a–d, red dashed lines).

After discarding the genes and cells using the three filters described above, we examined the remaining 5128 and 3992 gene–gene matrices of the α1 and α3 isoforms, respectively (Table S8). Using the *p* values of each gene–gene matrix, we computed their corresponding FDR adjusted *p* values. Figures 6a and 7a show volcano plots for the α1 and α3 isoform, respectively. Red color dots show the top 10 genes for each α isoform: α1 (*Chn2*, *Hpcal1*, *Nrgn*, *Neurod1*, *Selm*, *Kcnc1*, *Snrk*, *Snap25*, *Ckb*, and *Ccndbp1*) and α3 (*Sorcs3*, *Eml5*, *Neurod2*, *Ckb*, *Tbc1d4*, *Ptprz1*, *Pvrl1*, *Kirrel3*, *Pvalb*, and *Asic2*). These genes encode calcium-binding proteins (*Pvalb*, *Hpcal1*), calmodulin-binding protein (*Nrgn*), Cyclin D1 binding protein (*Ccndbp1*), transcriptional regulator proteins (*Neurod1*, *Neurod2*), membrane traffic proteins (*Sorcs3*, *Snap25*), kinase proteins (*Ckb*, *Snrk*, *Ptprz1*), GTPase-activating proteins (*Chn2*, *Tbc1d4*), adhesion molecule proteins (*Pvrl1*, *Kirrel3*), ion channel proteins (*Kcnc1*, *Asic2*), microtubule-associated protein (*Eml5*), and proteins with unknown functions (*Selm*). Interestingly, the calcium-binding protein parvalbumin encoded by *Pvalb*, one of the top genes co-expressed with the α3 isoform, is expressed in a subtype of GABAergic neurons expressing low Atp1a1 and high Atp1a3 α3 (Murata et al., 2020). In other studies, some of the proteins encoded by the genes identified have shown functions that might be related to a specific α isoform. For example, SNAP-25 encoded by *Snap25* gene, one of the top genes co-expressed with the α1 isoform, underlies the differences of the calcium responsiveness to depolarization between GABAergic and glutamatergic neurons (Verderio et al., 2004).

Given that gene expression and regulation is cell type-specific, it is conceivable that the correlation analysis with the α1 isoform is biased to the correlation exhibited by cerebellar granule cells. To test for this possibility, we reanalyzed the data excluding the cluster CB_1-1 and compared the outcomes under these two different conditions. The filtered subdataset for α1 enriched clusters was composed of 20,391 genes and 56,085 cells. After the three filters were performed, 5098 genes were selected (Table S8). The intersection between this output and the previous one is 5073 genes. By plotting the Spearman's correlation coefficients obtained from both analysis we observed a regression coefficient of 0.686, with a *p* value <2.2e-16 (Figure S6e), suggesting that cerebellar granule cells are not introducing bias.

To further explore the sets of co-expressing genes, we performed gene ontology analyses of the top 100 genes associated with each α isoform (Figures 6b and 7b, and Table S9 and S10), using ShinyGo software package (Ge et al., 2020) and DAVID (Huang da et al., 2009). Given that transcripts encoding α1 and α3 isoforms are expressed differently among neuronal populations, it is not surprising that there is some dissimilarity among the biological processes in which they might be involved. Even though the main known function of both isoforms is to transport ions across the cell membrane, the α3 isoform seems to be consistently more represented in neuronal-specific biological processes. These observations add support to the idea that this isoform has functions beyond the transport of Na^+ and K^+ ions (Clausen et al., 2017).

4 | DISCUSSION

The aim of this study was to analyze the expression pattern of Na^+/K^+-ATPase subunits in the mouse brain, focusing on the neuron-specific isoform α3, which has been implicated in several neurological diseases. We identified the predominant Na^+/K^+-ATPase isoform combinations in multiple cell types and regions across the brain (Table 1–2, and Tables S5 and S6). We confirmed that the expression of α3 isoform is exclusive to neurons of the PNS and CNS. We expanded on previous work by defining the neuronal clusters with largest expression of α1 and α3 isoforms and discovered significant variation of expression among subpopulations of α-associated cell types. Moreover, we detected the genes whose expression correlated with α1 or α3 in these neuronal clusters. To our knowledge, this study is the first investigation to comprehensively address the similarities and differences of Na^+/K^+-ATPase isoforms in various neuronal clusters at the single-cell level throughout the adult mouse brain.

In addition to confirming that the α isoforms in CNS neurons are α1 and α3, we found that for the other subunits, the β1 isoform and *Fxyd6* and *Fxyd7* isoforms predominate. Supporting a role of these isoforms in neuronal function, both α1- and α3-associated diseases can involve CNS symptoms such as epilepsy and intellectual disability, as well as peripheral nerve degeneration with α1. The modulatory subunit *Fxyd6* is potentially associated with susceptibility to schizophrenia (Choudhury et al., 2007; Zhong et al., 2011). While there are

FIGURE 7 Genes correlated with the expression of α3. (a) Volcano plot of Spearman's correlation coefficients versus -log10 (FDR-adjusted *p* values). Each symbol represents one test gene. Top 10 genes with highest positive correlations are marked with red color. Spearman's correlation and the corresponding log10 transformed FDR-adjusted *p* values were described in Sections 2.4 and 3.5. (b) A hierarchical clustering tree that summarizes the significant biological processes. The sizes of the blue dots and their corresponding values refer to the Enrichment FDR for the specific biological process, calculated by ShinyGo software (see Section 2.5)

currently no known β1-associated diseases, this may be due to its ubiquitous expression throughout other organ systems. The negative correlation between α1 and α3 expression further supports the view that α3 is the primary functional α isoform in some neurons. Thus, the α1/β1 and α3/β1 enzyme complexes are appropriate targets for the study of Na^+/K^+-ATPase in CNS neurons.

Clustering analysis of highly α3-expressing neurons identified the specific neuronal subtypes and brain locations that may be most relevant in the study of α3's function in the CNS and disease pathology. In unsupervised analysis, the majority of these top α3-expressing clusters were found in the cerebellum, hippocampus, and brainstem (Table S6).

In the cerebellum, our analysis suggested Golgi cells (Cluster#: CB_4–2 and CBINH2) and cerebellum basket cells (Cluster#: CB_3-1, -2, -3, -4, and CBINH1) as α3-enriched clusters, which added support for previous evidence of α3 production in these cerebellar interneurons at mRNA and protein levels (Chauhan & Siegel, 1997; Hieber et al., 1989; Hieber et al., 1991; Ikeda et al., 2013). Our data also showed that cerebellar granule cells (Cluster#: CB_1-1 and CBGRC) seldom expressed α3, which was also consistent with previous findings about the lack of α3 in granule cells (Ikeda et al., 2013). Remarkably, our results indicated that, although α3 has been heavily studied as the isoform in cerebellar Purkinje cells, it was only expressed at the medium level among all CNS neuronal clusters. We observed that 14.6% Purkinje cells (Cluster#: CB_2-1) from 2-month-old mice and 52.4% Purkinje cells (Cluster#: CBPC) from P19-25 mice did not have detectable α3, which was consistent with the previous observation in Atp1a3-ZsGreen1 mice (2–3 months) carrying a fluorescent reporter that about 22.4%–47.3% neurons within Purkinje cell layer were ZsGreen1 negative (Dobretsov et al., 2019), suggesting that most but not all Purkinje cells express α3.

In the hippocampus, the primary α3-expressing population is thought to be parvalbumin-expressing interneurons and hilar cells (Dobretsov et al., 2019; Murata et al., 2020). For example, excessive ZsGreen1-labeled cells were observed in dentate gyrus, subiculum, and postsubiculum areas, while the majority of the neurons within the hippocampal pyramidal layer were ZsGreen1-negative in Atp1a3-ZsGreen1 mice (Dobretsov et al., 2019). Glutamatergic cells and parvalbumin-expressing GABAergic neurons in the hilus were shown to have the highest expression level of *Atp1a3* mRNA using fluorescent labeling mRNA probes (Murata et al., 2020). In line with this work, we found that hippocampal basket cells and neuronal populations from subiculum and postsubiculum were among the top clusters for α3 production. Moreover, these hippocampal basket cells (Cluster#: HC_1-6 and HC_1-7) expressed parvalbumin but not cholecystokinin. Therefore, they were very likely to be the GABAergic neurons which provide stable high-frequency inhibitory output onto their target cells (Bartos & Elgueta, 2012). Another two highly-expressing α3 clusters were two subtypes (Cluster#: HC_1-10 and HC_1-8) of oriens-lacunosum moleculare cells, which are considered key to the pathophysiology of epilepsy and the most vulnerable interneuron population in models of epilepsy (Dinocourt et al., 2003; Dugladze et al., 2007), a symptom for many AHC and RDP patients (Kansagra et al., 2013). Trilaminar cells (Cluster#: TEINH13), which are fast-spiking cells and strongly phase-locked with gamma oscillations (Gloveli et al., 2005), were also identified as one of the top clusters. Although glutamatergic neurons highly expressing α3 ($Vglut1^+$/$Atp1a3^+$ cells) were found in hilus (Murata et al., 2020), this neuronal population apparently was not recruited in these two scRNA-Seq databases. According to the datasets, the two glutamatergic neurons identified in dentate and hilus (Cluster#: HC_6-5 and HC_6-6) only have a moderate level of α3 production. Moreover, these neurons express a calcium-binding protein calretinin which is not detected in the $Vglut1^+$/$Atp1a3^+$ cells, suggesting that they are distinct neuronal subtypes.

Besides cerebellum and hippocampus, several α3-enriched populations were found in the brainstem. Notably, excitatory neurons including Cluster# HBGLU7 & HBGLU8 from tegmental reticular nucleus (TRN), Cluster# HBGLU6 from pontine gray (PG), Cluster# HBGLU5 from pontine reticular nucleus, caudal part (PRNc), Cluster# HBGLU4 from medial vestibular nucleus (MV) and nucleus prepositus (PRN), as well as inhibitory neurons including Cluster# HBINH5 from gigantocellular reticular nucleus (GRN) were some of the top clusters. In agreement with previous findings, these neuronal clusters are localized in the sub-regions found to have strong ZsGreen1 expression in Atp1a3-ZsGreen1 mice (Dobretsov et al., 2019). Contrary, a few predicted clusters in our analysis, such as Cluster# HBGLU9 from spinal nucleus of the trigeminal (SPV), Cluster# HBINH7 from superior olivary complex and Cluster# HBINH8 from SPV, were in the sub-regions with less ZsGreen1 expression (Dobretsov et al., 2019), where further investigation could be required.

Strikingly, the three major brain regions and the cell types we found to express α3 are heavily linked to the pathogenesis of α3-related neurological disorders. Brain hypoplasia and/or progressive atrophy, found in some patients with α3-related diseases, particularly affect the cerebellum, hippocampus, and brainstem (Paciorkowski et al., 2015; Prange et al., 2020; Saito et al., 1998; Sasaki et al., 2017). Within the cerebellum, our results identify multiple neuronal clusters including Purkinje cells that are relevant to the study of α3 activity. Consistent with this, cerebellar knockdown of α3 in mice has been shown to cause aberrant Purkinje cell output, leading to dystonia, a major symptom of α3-associated disorders (Fremont et al., 2015). Similarly, the hippocampus displays highest α3 expression among fast-firing interneurons, which is consistent with the finding in a mouse model that impaired inhibitory neurotransmission in the hippocampus likely causes α3-associated epilepsy (Hunanyan et al., 2018). Furthermore, neuropathology of a patient with hippocampal atrophy showed loss of CA1 neurons (Paciorkowski et al., 2015), which may be explained by excitotoxicity due to inadequate GABAergic inhibition. In the brainstem, we found that both excitatory and inhibitory neuronal populations express α3. This may explain abnormal eye movements in these patients, particularly the distinctive feature of nystagmus in one eye (Sweney et al., 2009; Yang et al., 2014), which suggests dysfunction of nuclei in the pons that control coordination of the two eyes (Bae et al., 2013; Pierrot-Deseilligny, 2011). Neuronal loss and gliosis have been observed in the brainstem in other patients

(Oblak et al., 2014). The strong coincidence between neuronal clusters enriched in α3 identified in our analysis and the brain regions impaired in patients with α3 related diseases emphasized that the normal function of α3 was essential for these brain regions. Our results at least partially explained why cerebellum, hippocampus, and brain stem were most vulnerable to Na^+/K^+-ATPase pump dysfunction caused by α3 mutations. The top clusters in our study define the specific subpopulations of neurons that are of potential importance for further investigation on the pathogenesis of α3-related diseases.

Unbiased analysis of genes highly correlated with α isoforms expression revealed several genes that have highest positive correlations with α1 or α3 expression (Figures 6 and 7, and Table S8). Creatine kinase B (*Ckb*) is the gene with the highest confidence in its correlation with the expression of both isoforms. Its function is to use adenosine triphosphate (ATP) for producing phosphocreatine (PCr), which serves as an energy reservoir for the prompt regeneration of ATP, especially in tissues rapidly utilizing ATP, such as brain. Considering that Na^+/K^+-ATPase α subunits are one of the largest ATP consumers in brain, the expression correlation between *Ckb* and α isoforms could be relevant to energy consumption. The proneuronal transcription factors *Neurod1* (Neuronal differentiation 1) and *Neurod2* (Neuronal differentiation 2) are intriguingly correlated with α1 and α3 isoforms, respectively, suggesting that neurons from different lineages may have distinct preference for α isoform expression. Moreover, *Neurod2* was documented to be essential for rodent cerebellum development (Pieper et al., 2019). Axons of *Neurod2*-deficient cerebellar basket cells failed to project their inhibitory terminals to Purkinje cells, and therefore functional inhibitory circuits could not be formed in the ML (Pieper et al., 2019). The correlation among α3 and *Neurod2* may be helpful to diagnose neuronal subtypes which are more susceptible to damage induced by pathogenic α3 mutations, or even fail to develop normally, leading to hypoplasia of the cerebellum in some patients (Prange et al., 2020). Comparing the gene ontology analysis for top α1- and α3-correlated genes shows overlap in expected pathways such as energy metabolism, but also extensive differences among other gene categories, suggesting that this analysis captured isoform-specific cell type associations and/or cellular functions of α subunits. While α1 isoform is largely correlated with ion transport (potassium ions in particular), α3 isoform tends towards participating in synapse organization and synaptic signaling.

Beyond the fact that pump function is compromised in Na^+/K^+-ATPase-related disorders, little is known about the cellular and physiological underpinnings of the observed clinical manifestations. Our bioinformatic analysis provides robust and detailed information on the expression profile of all pump isoforms across the CNS and suggests potential partners/pathways involved in the pathogenesis of Na^+/K^+-ATPase-related disorders. We believe this information could be highly valuable to guide future researchers in selecting the best cellular models to further understand the disease mechanism and in identifying new therapeutic targets. Future studies using transcriptional profiling datasets will lead to a deeper understanding of the genes involved in Na^+/K^+-ATPase function in the human nervous system.

ACKNOWLEDGMENTS

Song Jiao, Kory Johnson, Sho Yano, Cristina Moreno, and Miguel Holmgren were supported by the Intramural Research Program of the NIH (NINDS and NHGRI).

CONFLICT OF INTEREST

The authors declare no potential conflict of interest.

AUTHOR CONTRIBUTIONS

Song Jiao, Kory Johnson, and Miguel Holmgren designed the project. Song Jiao performed experiments and analyzed the data. Song Jiao and Kory Johnson wrote scripts for bioinformatic analysis. All authors contributed to discussions and preparation of the manuscript. Song Jiao, Sho Yano, Cristina Moreno, and Miguel Holmgren wrote the manuscript.

PEER REVIEW

The peer review history for this article is available at https://publons.com/publon/10.1002/cne.25234.

DATA AVAILABILITY STATEMENT

Data sharing is not applicable to this article as no new data were created or analyzed in this study.

ORCID

Song Jiao https://orcid.org/0000-0003-0496-6454
Kory Johnson https://orcid.org/0000-0002-6693-3378
Cristina Moreno https://orcid.org/0000-0002-0171-6022
Sho Yano https://orcid.org/0000-0002-4177-3064
Miguel Holmgren https://orcid.org/0000-0001-8285-4242

REFERENCES

Anselm, I. A., Sweadner, K. J., Gollamudi, S., Ozelius, L. J., & Darras, B. T. (2009). Rapid-onset dystonia-parkinsonism in a child with a novel atp1a3 gene mutation. *Neurology*, *73*(5), 400–401. https://doi.org/10.1212/WNL.0b013e3181b04acd

Arystarkhova, E., & Sweadner, K. J. (1996). Isoform-specific monoclonal antibodies to Na,K-ATPase alpha subunits. Evidence for a tissue-specific post-translational modification of the alpha subunit. *J Biol Chem*, *271*(38), 23407–23417. https://doi.org/10.1074/jbc.271.38.23407

Arystarkhova, E., & Sweadner, K. J. (1997). Tissue-specific expression of the Na,K-ATPase beta3 subunit. The presence of beta3 in lung and liver addresses the problem of the missing subunit. *The Journal of Biological Chemistry*, *272*(36), 22405–22408. https://doi.org/10.1074/jbc.272.36.22405

Arystarkhova, E., Wetzel, R. K., Asinovski, N. K., & Sweadner, K. J. (1999). The gamma subunit modulates Na^+ and K^+ affinity of the renal Na,K-ATPase. *The Journal of Biological Chemistry*, *274*(47), 33183–33185. https://doi.org/10.1074/jbc.274.47.33183

Azarias, G., Kruusmagi, M., Connor, S., Akkuratov, E. E., Liu, X. L., Lyons, D., Brismar, H., Broberger, C., & Aperia, A. (2013). A specific and essential role for Na,K-ATPase alpha3 in neurons co-expressing alpha1 and alpha3. *The Journal of Biological Chemistry*, *288*(4), 2734–2743. https://doi.org/10.1074/jbc.M112.425785

Bae, Y. J., Kim, J. H., Choi, B. S., Jung, C., & Kim, E. (2013). Brainstem pathways for horizontal eye movement: Pathologic correlation with MR imaging. *Radiographics*, *33*(1), 47–59. https://doi.org/10.1148/rg.331125033

Bartos, M., & Elgueta, C. (2012). Functional characteristics of parvalbumin- and cholecystokinin-expressing basket cells. *The Journal of Physiology*, *590*(4), 669–681. https://doi.org/10.1113/jphysiol.2011.226175

Beguin, P., Crambert, G., Monnet-Tschudi, F., Uldry, M., Horisberger, J. D., Garty, H., & Geering, K. (2002). FXYD7 is a brain-specific regulator of Na,K-ATPase alpha 1-beta isozymes. *The EMBO Journal*, *21*(13), 3264–3273. https://doi.org/10.1093/emboj/cdf330

Benjamini, Y., Heller, R., & Yekutieli, D. (2009). Selective inference in complex research. *Philosophical Transactions of the Royal Society A-Mathematical Physical and Engineering Sciences*, *367*(1906), 4255–4271.

Blanco, G., & Mercer, R. W. (1998). Isozymes of the Na-K-ATPase: Heterogeneity in structure, diversity in function. *The American Journal of Physiology*, *275*(5), F633–F650. https://doi.org/10.1152/ajprenal.1998.275.5.F633

Bottger, P., Tracz, Z., Heuck, A., Nissen, P., Romero-Ramos, M., & Lykke-Hartmann, K. (2011). Distribution of Na/K-ATPase alpha 3 isoform, a sodium-potassium P-type pump associated with rapid-onset of dystonia parkinsonism (RDP) in the adult mouse brain. *The Journal of Comparative Neurology*, *519*(2), 376–404. https://doi.org/10.1002/cne.22524

Brashear, A., Dobyns, W. B., de Carvalho Aguiar, P., Borg, M., Frijns, C. J., Gollamudi, S., Green, A., Guimaraes, J., Haake, B. C., Klein, C., Linazasoro, G., Münchau, A., Raymond, D., Riley, D., Saunders-Pullman, R., Tijssen, M. A. J., Webb, D., Zaremba, J., Bressman, S. B., & Ozelius, L. J. (2007). The phenotypic spectrum of rapid-onset dystonia-parkinsonism (RDP) and mutations in the ATP1A3 gene. *Brain*, *130*(Pt 3), 828–835. https://doi.org/10.1093/brain/awl340

Cameron, R., Klein, L., Shyjan, A. W., Rakic, P., & Levenson, R. (1994). Neurons and astroglia express distinct subsets of Na,K-ATPase alpha and beta subunits. *Brain Research. Molecular Brain Research*, *21*(3–4), 333–343. https://doi.org/10.1016/0169-328x(94)90264-x

Chauhan, N., & Siegel, G. (1997). Differential expression of Na,K-ATPase alpha-isoform mRNAs in aging rat cerebellum. *Journal of Neuroscience Research*, *47*(3), 287–299.

Choudhury, K., McQuillin, A., Puri, V., Pimm, J., Datta, S., Thirumalai, S., Krasucki, R., Lawrence, J., Bass, N. J., Quested, D., Crombie, C., Fraser, G., Walker, N., Nadeem, H., Johnson, S., Curtis, D., St. Clair, D., & Gurling, H. M. (2007). A genetic association study of chromosome 11q22-24 in two different samples implicates the FXYD6 gene, encoding phosphohippolin, in susceptibility to schizophrenia. *American Journal of Human Genetics*, *80*(4), 664–672. https://doi.org/10.1086/513475

Clapcote, S. J., Duffy, S., Xie, G., Kirshenbaum, G., Bechard, A. R., Rodacker Schack, V., Petersen, J., Sinai, L., Saab, B. J., Lerch, J. P., Minassian, B. A., Ackerley, C. A., Sled, J. G., Cortez, M. A., Henderson, J. T., Vilsen, B., & Roder, J. C. (2009). Mutation I810N in the alpha3 isoform of Na^+,K^+-ATPase causes impairments in the sodium pump and hyperexcitability in the CNS. *Proceedings of the National Academy of Sciences of the United States of America*, *106*(33), 14085–14090. https://doi.org/10.1073/pnas.0904817106

Clausen, M. V., Hilbers, F., & Poulsen, H. (2017). The structure and function of the Na,K-ATPase isoforms in health and disease. *Frontiers in Physiology*, *8*, 371. https://doi.org/10.3389/fphys.2017.00371

de Carvalho Aguiar, P., Sweadner, K. J., Penniston, J. T., Zaremba, J., Liu, L., Caton, M., Linazasoro, G., Borg, M., Tijssen, M. A. J., Bressman, S. B., Dobyns, W. B., Brashear, A., & Ozelius, L. J. (2004). Mutations in the Na^+/K^+-ATPase alpha3 gene ATP1A3 are associated with rapid-onset dystonia parkinsonism. *Neuron*, *43*(2), 169–175. https://doi.org/10.1016/j.neuron.2004.06.028

de Lores Arnaiz, G. R., & Ordieres, M. G. (2014). Brain Na^+, K^+-ATPase activity in aging and disease. *International Journal of Biomedical Sciences*, *10*(2), 85–102.

DeAndrade, M. P., Yokoi, F., van Groen, T., Lingrel, J. B., & Li, Y. (2011). Characterization of Atp1a3 mutant mice as a model of rapid-onset dystonia with parkinsonism. *Behavioural Brain Research*, *216*(2), 659–665. https://doi.org/10.1016/j.bbr.2010.09.009

Delprat, B., Schaer, D., Roy, S., Wang, J., Puel, J. L., & Geering, K. (2007). FXYD6 is a novel regulator of Na,K-ATPase expressed in the inner ear. *The Journal of Biological Chemistry*, *282*(10), 7450–7456. https://doi.org/10.1074/jbc.M609872200

Demos, M. K., van Karnebeek, C. D., Ross, C. J., Adam, S., Shen, Y., Zhan, S. H., Shyr, C., Horvath, G., Suri, M., Fryer, A., Jones, S. J., Friedman, J. M., & FORGE Canada Consortium. (2014). A novel recurrent mutation in ATP1A3 causes CAPOS syndrome. *Orphanet Journal of Rare Diseases*, *9*, 15. https://doi.org/10.1186/1750-1172-9-15

Dinocourt, C., Petanjek, Z., Freund, T. F., Ben-Ari, Y., & Esclapez, M. (2003). Loss of interneurons innervating pyramidal cell dendrites and axon initial segments in the CA1 region of the hippocampus following pilocarpine-induced seizures. *The Journal of Comparative Neurology*, *459*(4), 407–425. https://doi.org/10.1002/cne.10622

Dobretsov, M., Hayar, A., Kockara, N. T., Kozhemyakin, M., Light, K. E., Patyal, P., Pierce, D. R., & Wight, P. A. (2019). A transgenic mouse model to selectively identify α3 Na,K-ATPase expressing cells in the nervous system. *Neuroscience*, *398*, 274–294. https://doi.org/10.1016/j.neuroscience.2018.07.018

Dugladze, T., Vida, I., Tort, A. B., Gross, A., Otahal, J., Heinemann, U., Kopell, N. J., & Gloveli, T. (2007). Impaired hippocampal rhythmogenesis in a mouse model of mesial temporal lobe epilepsy. *Proceedings of the National Academy of Sciences of the United States of America*, *104*(44), 17530–17535. https://doi.org/10.1073/pnas.0708301104

Edwards, I. J., Bruce, G., Lawrenson, C., Howe, L., Clapcote, S. J., Deuchars, S. A., & Deuchars, J. (2013). Na^+/K^+ ATPase alpha1 and alpha3 isoforms are differentially expressed in alpha- and gamma-motoneurons. *The Journal of Neuroscience*, *33*(24), 9913–9919. https://doi.org/10.1523/JNEUROSCI.5584-12.2013

Fremont, R., Tewari, A., & Khodakhah, K. (2015). Aberrant Purkinje cell activity is the cause of dystonia in a shRNA-based mouse model of rapid onset dystonia-parkinsonism. *Neurobiology of Disease*, *82*, 200–212. https://doi.org/10.1016/j.nbd.2015.06.004

Ge, S. X., Jung, D., & Yao, R. (2020). ShinyGO: A graphical gene-set enrichment tool for animals and plants. *Bioinformatics*, *36*(8), 2628–2629. https://doi.org/10.1093/bioinformatics/btz931

Geering, K. (2005). Function of FXYD proteins, regulators of Na, K-ATPase. *Journal of Bioenergetics and Biomembranes*, *37*(6), 387–392. https://doi.org/10.1007/s10863-005-9476-x

Gloveli, T., Dugladze, T., Saha, S., Monyer, H., Heinemann, U., Traub, R. D., Whittington, M. A., & Buhl, E. H. (2005). Differential involvement of oriens/pyramidale interneurones in hippocampal network oscillations in vitro. *The Journal of Physiology*, *562*(Pt 1), 131–147. https://doi.org/10.1113/jphysiol.2004.073007

Gritz, S. M., & Radcliffe, R. A. (2013). Genetic effects of ATP1A2 in familial hemiplegic migraine type II and animal models. *Human Genomics*, *7*, 8. https://doi.org/10.1186/1479-7364-7-8

Harada, K., Lin, H., Endo, Y., Fujishiro, N., Sakamoto, Y., & Inoue, M. (2006). Subunit composition and role of Na^+,K^+-ATPases in ventricular myocytes. *The Journal of Physiological Sciences*, *56*(1), 113–121. https://doi.org/10.2170/physiolsci.rp001905

He, J., Guo, L., Lin, S., Chen, W., Xu, G., Cai, B., Xu, L., Hong, J., Qiu, L., Wang, N., & Chen, W. (2019). ATP1A1 mutations cause intermediate Charcot-Marie-Tooth disease. *Human Mutation*, *40*(12), 2334–2343. https://doi.org/10.1002/humu.23886

Heimer, G., Sadaka, Y., Israelian, L., Feiglin, A., Ruggieri, A., Marshall, C. R., Scherer, S. W., Ganelin-Cohen, E., Marek-Yagel, D., Tzadok, M., Nissenkorn, A., Anikster, Y., Minassian, B. A., & Zeev, B. B. (2015). CAOS-episodic cerebellar ataxia, areflexia, optic atrophy, and sensorineural hearing loss: A third allelic disorder of the ATP1A3 gene. *Journal of Child Neurology*, *30*(13), 1749–1756. https://doi.org/10.1177/0883073815579708

Heinzen, E. L., Swoboda, K. J., Hitomi, Y., Gurrieri, F., Nicole, S., de Vries, B., Tiziano, F. D., Fontaine, B., Walley, N. M., Heavin, S., Panagiotakaki, E., Fiori, S., Abiusi, E., Di Pietro, L., Sweney, M. T., Newcomb, T. M., Viollet, L., Huff, C., Jorde, L. B., … Goldstein, D. B. (2012). De novo mutations in ATP1A3 cause alternating hemiplegia of childhood. *Nature Genetics*, *44*(9), 1030–1034. https://doi.org/10.1038/ng.2358

Hieber, V., Siegel, G. J., Desmond, T., Liu, J. L., & Ernst, S. A. (1989). Na, K-ATPase: comparison of the cellular localization of alpha-subunit mRNA and polypeptide in mouse cerebellum, retina, and kidney. *Journalof Neuroscience Research*, *23*(1), 9–20. https://doi.org/10.1002/jnr.490230103

Hieber, V., Siegel, G. J., Fink, D. J., Beaty, M. W., & Mata, M. (1991). Differential distribution of (Na, K)-ATPase alpha isoforms in the central nervous system. *Cellular and Molecular Neurobiology*, *11*(2), 253–262. https://doi.org/10.1007/BF00769038

Hoei-Hansen, C. E., Dali, C. I., Lyngbye, T. J., Duno, M., & Uldall, P. (2014). Alternating hemiplegia of childhood in Denmark: Clinical manifestations and ATP1A3 mutation status. *European Journal of Paediatric Neurology*, *18*(1), 50–54. https://doi.org/10.1016/j.ejpn.2013.08.007

Hou, R., Denisenko, E., & Forrest, A. R. R. (2019). scMatch: A single-cell gene expression profile annotation tool using reference datasets. *Bioinformatics*, *35*(22), 4688–4695. https://doi.org/10.1093/bioinformatics/btz292

Huang da, W., Sherman, B. T., & Lempicki, R. A. (2009). Systematic and integrative analysis of large gene lists using DAVID bioinformatics resources. *Nature Protocols*, *4*(1), 44–57. https://doi.org/10.1038/nprot.2008.211

Hunanyan, A. S., Fainberg, N. A., Linabarger, M., Arehart, E., Leonard, A. S., Adil, S. M., Helseth, A. R., Swearingen, A. K., Forbes, S. L., Rodriguiz, R. M., Rhodes, T., Yao, X., Kibbi, N., Hochman, D. W., Wetsel, W. C., Hochgeschwender, U., & Mikati, M. A. (2015). Knock-in mouse model of alternating hemiplegia of childhood: Behavioral and electrophysiologic characterization. *Epilepsia*, *56*(1), 82–93. https://doi.org/10.1111/epi.12878

Hunanyan, A. S., Helseth, A. R., Abdelnour, E., Kherallah, B., Sachdev, M., Chung, L., Masoud, M., Richardson, J., Li, Q., Nadler, J. V., Moore, S. D., & Mikati, M. A. (2018). Mechanisms of increased hippocampal excitability in the Mashl(+/−) mouse model of Na(+)/K(+)-ATPase dysfunction. *Epilepsia*, *59*(7), 1455–1468. https://doi.org/10.1111/epi.14441

Ikeda, K., Onimaru, H., & Kawakami, K. (2017). Knockout of sodium pump alpha3 subunit gene (Atp1a3(-/-)) results in perinatal seizure and defective respiratory rhythm generation. *Brain Research*, *1666*, 27–37. https://doi.org/10.1016/j.brainres.2017.04.014

Ikeda, K., Satake, S., Onaka, T., Sugimoto, H., Takeda, N., Imoto, K., & Kawakami, K. (2013). Enhanced inhibitory neurotransmission in the cerebellar cortex of Atp1a3-deficient heterozygous mice. *The Journal of Physiology*, *591*(13), 3433–3449. https://doi.org/10.1113/jphysiol.2012.247817

Ilicic, T., Kim, J. K., Kolodziejczyk, A. A., Bagger, F. O., McCarthy, D. J., Marioni, J. C., & Teichmann, S. A. (2016). Classification of low quality cells from single-cell RNA-seq data. *Genome Biology*, *17*, 29. https://doi.org/10.1186/s13059-016-0888-1

Isaksen, T. J., Kros, L., Vedovato, N., Holm, T. H., Vitenzon, A., Gadsby, D. C., Khodakhah, K., & Lykke-Hartmann, K. (2017). Hypothermia-induced dystonia and abnormal cerebellar activity in a mouse model with a single disease-mutation in the sodium-potassium pump. *PLoS Genetics*, *13*(5), e1006763. https://doi.org/10.1371/journal.pgen.1006763

Jaisser, F., Canessa, C. M., Horisberger, J. D., & Rossier, B. C. (1992). Primary sequence and functional expression of a novel ouabain-resistant Na,K-ATPase. The beta subunit modulates potassium activation of the Na,K-pump. *The Journal of Biological Chemistry*, *267*(24), 16895–16903.

Jimenez, T., McDermott, J. P., Sanchez, G., & Blanco, G. (2011). Na,K-ATPase alpha4 isoform is essential for sperm fertility. *Proceedings of the National Academy of Sciences of the United States of America*, *108*(2), 644–649. https://doi.org/10.1073/pnas.1016902108

Jimenez, T., Sanchez, G., McDermott, J. P., Nguyen, A. N., Kumar, T. R., & Blanco, G. (2011). Increased expression of the Na,K-ATPase alpha4 isoform enhances sperm motility in transgenic mice. *Biology of Reproduction*, *84*(1), 153–161. https://doi.org/10.1095/biolreprod.110.087064

Kadowaki, K., Sugimoto, K., Yamaguchi, F., Song, T., Watanabe, Y., Singh, K., & Tokuda, M. (2004). Phosphohippolin expression in the rat central nervous system. *Brain Research. Molecular Brain Research*, *125*(1–2), 105–112. https://doi.org/10.1016/j.molbrainres.2004.03.021

Kansagra, S., Mikati, M. A., & Vigevano, F. (2013). Alternating hemiplegia of childhood. *Handbook of Clinical Neurology*, *112*, 821–826. https://doi.org/10.1016/B978-0-444-52910-7.00001-5

Kirshenbaum, G. S., Clapcote, S. J., Duffy, S., Burgess, C. R., Petersen, J., Jarowek, K. J., Yucel, Y. H., Cortez, M. A., Snead, O. C., Vilsen, B., Peever, J. H., Ralph, M. R., & Roder, J. C. (2011). Mania-like behavior induced by genetic dysfunction of the neuron-specific Na^+,K^+-ATPase alpha3 sodium pump. *Proceedings of the National Academy of Sciences of the United States of America*, *108*(44), 18144–18149. https://doi.org/10.1073/pnas.1108416108

Kirshenbaum, G. S., Saltzman, K., Rose, B., Petersen, J., Vilsen, B., & Roder, J. C. (2011). Decreased neuronal Na^+, K^+ -ATPase activity in Atp1a3 heterozygous mice increases susceptibility to depression-like endophenotypes by chronic variable stress. *Genes, Brain, and Behavior*, *10*(5), 542–550. https://doi.org/10.1111/j.1601-183X.2011.00691.x

Korbo, L., Andersen, B. B., Ladefoged, O., & Moller, A. (1993). Total numbers of various cell types in rat cerebellar cortex estimated using an unbiased stereological method. *Brain Research*, *609*(1–2), 262–268. https://doi.org/10.1016/0006-8993(93)90881-m

Lassuthova, P., Rebelo, A. P., Ravenscroft, G., Lamont, P. J., Davis, M. R., Manganelli, F., Feely, S. M., Bacon, C., Brožková, D. Š., Haberlova, J., Mazanec, R., Tao, F., Saghira, C., Abreu, L., Courel, S., Powell, E., Buglo, E., Bis, D. M., Baxter, M. F., … Zuchner, S. (2018). Mutations in ATP1A1 cause dominant Charcot-Marie-tooth type 2. *American Journal of Human Genetics*, *102*(3), 505–514. https://doi.org/10.1016/j.ajhg.2018.01.023

Lecuona, E., Luquin, S., Avila, J., Garcia-Segura, L. M., & Martin-Vasallo, P. (1996). Expression of the beta 1 and beta 2(AMOG) subunits of the Na,K-ATPase in neural tissues: cellular and developmental distribution patterns. *Brain Research Bulletin*, *40*(3), 167–174. https://doi.org/10.1016/0361-9230(96)00042-1

Lee, J. Y., Gollamudi, S., Ozelius, L. J., Kim, J. Y., & Jeon, B. S. (2007). ATP1A3 mutation in the first asian case of rapid-onset dystonia-parkinsonism. *Movement Disorders*, *22*(12), 1808–1809. https://doi.org/10.1002/mds.21638

Lingrel, J. B., Orlowski, J., Shull, M. M., & Price, E. M. (1990). Molecular genetics of Na,K-ATPase. *Progress in Nucleic Acid Research and Molecular Biology*, *38*, 37–89. https://doi.org/10.1016/s0079-6603(08)60708-4

Lutsenko, S., & Kaplan, J. H. (1993). An essential role for the extracellular domain of the Na,K-ATPase beta-subunit in cation occlusion. *Biochemistry*, *32*(26), 6737–6743. https://doi.org/10.1021/bi00077a029

Maas, R. P., Schieving, J. H., Schouten, M., Kamsteeg, E. J., & van de Warrenburg, B. P. (2016). The genetic homogeneity of CAPOS syndrome: Four new patients with the c.2452G>a (p.Glu818Lys) mutation in the ATP1A3 gene. *Pediatric Neurology*, *59*, 71–75.e1. https://doi.org/10.1016/j.pediatrneurol.2016.02.010

McDermott, J. P., Sanchez, G., Chennathukuzhi, V., & Blanco, G. (2012). Green fluorescence protein driven by the Na,K-ATPase alpha4 isoform promoter is expressed only in male germ cells of mouse testis. *Journal of Assisted Reproduction and Genetics*, *29*(12), 1313–1325. https://doi.org/10.1007/s10815-012-9876-x

McGrail, K. M., Phillips, J. M., & Sweadner, K. J. (1991). Immunofluorescent localization of three Na,K-ATPase isozymes in the rat central nervous

system: Both neurons and glia can express more than one Na,K-ATPase. *The Journal of Neuroscience*, *11*(2), 381–391.

McKeon, A., Ozelius, L. J., Hardiman, O., Greenway, M. J., & Pittock, S. J. (2007). Heterogeneity of presentation and outcome in the Irish rapid-onset dystonia-parkinsonism kindred. *Movement Disorders*, *22*(9), 1325–1327. https://doi.org/10.1002/mds.21335

Mercer, R. W., Biemesderfer, D., Bliss, D. P., Jr., Collins, J. H., & Forbush, B., 3rd. (1993). Molecular cloning and immunological characterization of the gamma polypeptide, a small protein associated with the Na,K-ATPase. *The Journal of Cell Biology*, *121*(3), 579–586. https://doi.org/10.1083/jcb.121.3.579

Morth, J. P., Pedersen, B. P., Toustrup-Jensen, M. S., Sorensen, T. L., Petersen, J., Andersen, J. P., Vilsen, B., & Nissen, P. (2007). Crystal structure of the sodium-potassium pump. *Nature*, *450*(7172), 1043–1049. https://doi.org/10.1038/nature06419

Moseley, A. E., Williams, M. T., Schaefer, T. L., Bohanan, C. S., Neumann, J. C., Behbehani, M. M., Vorhees, C. V., & Lingrel, J. B. (2007). Deficiency in Na,K-ATPase alpha isoform genes alters spatial learning, motor activity, and anxiety in mice. *The Journal of Neuroscience*, *27*(3), 616–626. https://doi.org/10.1523/JNEUROSCI.4464-06.2007

Murata, K., Kinoshita, T., Ishikawa, T., Kuroda, K., Hoshi, M., & Fukazawa, Y. (2020). Region- and neuronal-subtype-specific expression of Na,K-ATPase alpha and beta subunit isoforms in the mouse brain. *The Journal of Comparative Neurology*, *528*(16), 2654–2678. https://doi.org/10.1002/cne.24924

Oblak, A. L., Hagen, M. C., Sweadner, K. J., Haq, I., Whitlow, C. T., Maldjian, J. A., Epperson, F., Cook, J. F., Stacy, M., Murrell, J. R., Ozelius, L. J., Brashear, A., & Ghetti, B. (2014). Rapid-onset dystonia-parkinsonism associated with the I758S mutation of the ATP1A3 gene: A neuropathologic and neuroanatomical study of four siblings. *Acta Neuropathologica*, *128*(1), 81–98. https://doi.org/10.1007/s00401-014-1279-x

Paciorkowski, A. R., McDaniel, S. S., Jansen, L. A., Tully, H., Tuttle, E., Ghoneim, D. H., Tupal, S., Gunter, S. A., Vasta, V., Zhang, Q., Tran, T., Liu, Y. B., Ozelius, L. J., Brashear, A., Sweadner, K. J., Dobyns, W. B., & Hahn, S. (2015). Novel mutations in ATP1A3 associated with catastrophic early life epilepsy, episodic prolonged apnea, and postnatal microcephaly. *Epilepsia*, *56*(3), 422–430. https://doi.org/10.1111/epi.12914

Panagiotakaki, E., Gobbi, G., Neville, B., Ebinger, F., Campistol, J., Nevsimalova, S., Laan, L., Casaer, P., Spiel, G., Giannotta, M., Fons, C., Ninan, M., Sange, G., Schyns, T., Vavassori, R., Poncelin, D., ENRAH Consortium, & Arzimanoglou, A. (2010). Evidence of a non-progressive course of alternating hemiplegia of childhood: Study of a large cohort of children and adults. *Brain*, *133*(Pt 12), 3598–3610. https://doi.org/10.1093/brain/awq295

Peng, L., Martin-Vasallo, P., & Sweadner, K. J. (1997). Isoforms of Na,K-ATPase alpha and beta subunits in the rat cerebellum and in granule cell cultures. *The Journal of Neuroscience*, *17*(10), 3488–3502.

Picton, L. D., Nascimento, F., Broadhead, M. J., Sillar, K. T., & Miles, G. B. (2017). Sodium pumps mediate activity-dependent changes in mammalian motor networks. *The Journal of Neuroscience*, *37*(4), 906–921. https://doi.org/10.1523/JNEUROSCI.2005-16.2016

Pieper, A., Rudolph, S., Wieser, G. L., Gotze, T., Miessner, H., Yonemasu, T., Yan, K., Tzvetanova, I., Castillo, B. D., Bode, U., Bormuth, I., Wadiche, J. I., Schwab, M. H., & Goebbels, S. (2019). NeuroD2 controls inhibitory circuit formation in the molecular layer of the cerebellum. *Scientific Reports*, *9*(1), 1448. https://doi.org/10.1038/s41598-018-37850-7

Pierrot-Deseilligny, C. (2011). Nuclear, internuclear, and supranuclear ocular motor disorders. *Handbook of Clinical Neurology*, *102*, 319–331. https://doi.org/10.1016/B978-0-444-52903-9.00018-2

Prange, L., Pratt, M., Herman, K., Schiffmann, R., Mueller, D. M., McLean, M., Mendez, M. M., Walley, N., Heinzen, E. L., Goldstein, D., Shashi, V., Hunanyan, A., Pagadala, V., & Mikati, M. A. (2020). D-DEMO, a distinct phenotype caused by ATP1A3 mutations. *Neurology Genetics*, *6*(5), e466. https://doi.org/10.1212/NXG.0000000000000466

Richards, K. S., Bommert, K., Szabo, G., & Miles, R. (2007). Differential expression of Na^+/K^+-ATPase alpha-subunits in mouse hippocampal interneurones and pyramidal cells. *The Journal of Physiology*, *585*(Pt 2), 491–505. https://doi.org/10.1113/jphysiol.2007.144733

Rodacker, V., Toustrup-Jensen, M., & Vilsen, B. (2006). Mutations Phe785-Leu and Thr618Met in Na^+,K^+-ATPase, associated with familial rapid-onset dystonia parkinsonism, interfere with Na+ interaction by distinct mechanisms. *The Journal of Biological Chemistry*, *281*(27), 18539–18548. https://doi.org/10.1074/jbc.M601780200

Rosewich, H., Thiele, H., Ohlenbusch, A., Maschke, U., Altmuller, J., Frommolt, P., Zirn, B., Ebinger, F., Siemes, H., Nürnberg, P., Brockmann, K., & Gartner, J. (2012). Heterozygous de-novo mutations in ATP1A3 in patients with alternating hemiplegia of childhood: A whole-exome sequencing gene-identification study. *Lancet Neurology*, *11*(9), 764–773. https://doi.org/10.1016/S1474-4422(12)70182-5

Saito, Y., Sakuragawa, N., Sasaki, M., Sugai, K., & Hashimoto, T. (1998). A case of alternating hemiplegia of childhood with cerebellar atrophy. *Pediatric Neurology*, *19*(1), 65–68. https://doi.org/10.1016/s0887-8994(98)00016-2

Sasaki, M., Ishii, A., Saito, Y., & Hirose, S. (2017). Progressive brain atrophy in alternating hemiplegia of childhood. *Movement Disorders Clinical Practice*, *4*(3), 406–411. https://doi.org/10.1002/mdc3.12451

Saunders, A., Macosko, E. Z., Wysoker, A., Goldman, M., Krienen, F. M., de Rivera, H., Bien, E., Baum, M., Bortolin, L., Wang, S., Goeva, A., Nemesh, J., Kamitaki, N., Brumbaugh, S., Kulp, D., & McCarroll, S. A. (2018). Molecular diversity and specializations among the cells of the adult mouse brain. *Cell*, *174*(4), 1015–1030.e16. https://doi.org/10.1016/j.cell.2018.07.028

Schlingmann, K. P., Bandulik, S., Mammen, C., Tarailo-Graovac, M., Holm, R., Baumann, M., König, J., Lee, J. J. Y., Drögemöller, B., Imminger, K., Beck, B. B., Altmüller, J., Thiele, H., Waldegger, S., van't Hoff, W., Kleta, R., Warth, R., van Karnebeek, C. D. M., Vilsen, B., … Konrad, M. (2018). Germline de novo mutations in ATP1A1 cause renal hypomagnesemia, refractory seizures, and intellectual disability. *American Journal of Human Genetics*, *103*(5), 808–816. https://doi.org/10.1016/j.ajhg.2018.10.004

Schneider, J. W., Mercer, R. W., Caplan, M., Emanuel, J. R., Sweadner, K. J., Benz, E. J., Jr., & Levenson, R. (1985). Molecular cloning of rat brain Na,K-ATPase alpha-subunit cDNA. *Proceedings of the National Academy of Sciences of the United States of America*, *82*(18), 6357–6361. https://doi.org/10.1073/pnas.82.18.6357

Shamraj, O. I., & Lingrel, J. B. (1994). A putative fourth Na^+,K^+-ATPase alpha-subunit gene is expressed in testis. *Proceedings of the National Academy of Sciences of the United States of America*, *91*(26), 12952–12956. https://doi.org/10.1073/pnas.91.26.12952

Shinoda, T., Ogawa, H., Cornelius, F., & Toyoshima, C. (2009). Crystal structure of the sodium-potassium pump at 2.4 A resolution. *Nature*, *459*(7245), 446–450. https://doi.org/10.1038/nature07939

Shull, G. E., Greeb, J., & Lingrel, J. B. (1986). Molecular cloning of three distinct forms of the Na^+,K^+-ATPase alpha-subunit from rat brain. *Biochemistry*, *25*(25), 8125–8132. https://doi.org/10.1021/bi00373a001

Shull, G. E., Lane, L. K., & Lingrel, J. B. (1986). Amino-acid sequence of the beta-subunit of the $(Na^+ + K^+)$ATPase deduced from a cDNA. *Nature*, *321*(6068), 429–431. https://doi.org/10.1038/321429a0

Stregapede, F., Travaglini, L., Rebelo, A. P., Cintra, V. P., Bellacchio, E., Bosco, L., Alfieri, P., Pro, S., Zuchner, S., Bertini, E., & Nicita, F. (2020). Hereditary spastic paraplegia is a novel phenotype for germline de novo ATP1A1 mutation. *Clinical Genetics*, *97*(3), 521–526. https://doi.org/10.1111/cge.13668

Stuart, T., Butler, A., Hoffman, P., Hafemeister, C., Papalexi, E., Mauck, W. M., 3rd, Hao, Y., Stoeckius, M., Smibert, P., & Satija, R. (2019). Comprehensive integration of single-cell data. *Cell*, *177*(7), 1888–1902.e21. https://doi.org/10.1016/j.cell.2019.05.031

Sweadner, K. J. (1991). Overview: Subunit diversity in the Na,K-ATPase. *Society of General Physiologists Series*, *46*, 63–76.

Sweadner, K. J., & Rael, E. (2000). The FXYD gene family of small ion transport regulators or channels: cDNA sequence, protein signature sequence, and expression. *Genomics*, *68*(1), 41–56. https://doi.org/10.1006/geno.2000.6274

Sweney, M. T., Silver, K., Gerard-Blanluet, M., Pedespan, J. M., Renault, F., Arzimanoglou, A., Schlesinger-Massart, M., Lewelt, A. J., Reyna, S. P., & Swoboda, K. J. (2009). Alternating hemiplegia of childhood: Early characteristics and evolution of a neurodevelopmental syndrome. *Pediatrics*, *123*(3), e534–e541. https://doi.org/10.1542/peds.2008-2027

Szekely, G. J., & Rizzo, M. L. (2005). Hierarchical clustering via joint between-within distances: Extending Ward's minimum variance method. *Journal of Classification*, *22*(2), 151–183. https://doi.org/10.1007/s00357-005-0012-9

Takeyasu, K., Tamkun, M. M., Renaud, K. J., & Fambrough, D. M. (1988). Ouabain-sensitive (Na+ + K+)-ATPase activity expressed in mouse L cells by transfection with DNA encoding the alpha-subunit of an avian sodium pump. *The Journal of Biological Chemistry*, *263*(9), 4347–4354.

Team, R. C. (2019). R: A language and environment for statistical computing. R Foundation for Statistical Computing, Vienna, Austria.

Vanmolkot, K. R., Kors, E. E., Turk, U., Turkdogan, D., Keyser, A., Broos, L. A., Kia, S. K., van den Heuvel, J. J. M. W., Black, D. F., Haan, J., Frants, R. R., Barone, V., Ferrari, M. D., Casari, G., Koenderink, J. B., & van den Maagdenberg, A. M. (2006). Two de novo mutations in the Na,K-ATPase gene ATP1A2 associated with pure familial hemiplegic migraine. *European Journal of Human Genetics*, *14*(5), 555–560. https://doi.org/10.1038/sj.ejhg.5201607

Verderio, C., Pozzi, D., Pravettoni, E., Inverardi, F., Schenk, U., Coco, S., Proux-Gillardeaux, V., Galli, T., Rossetto, O., Frassoni, C., & Matteoli, M. (2004). SNAP-25 modulation of calcium dynamics underlies differences in GABAergic and glutamatergic responsiveness to depolarization. *Neuron*, *41*(4), 599–610. https://doi.org/10.1016/s0896-6273(04)00077-7

Watts, A. G., Sanchez-Watts, G., Emanuel, J. R., & Levenson, R. (1991). Cell-specific expression of mRNAs encoding Na+,K(+)-ATPase alpha- and beta-subunit isoforms within the rat central nervous system. *Proceedings of the National Academy of Sciences of the United States of America*, *88*(16), 7425–7429. https://doi.org/10.1073/pnas.88.16.7425

Yang, X., Gao, H., Zhang, J., Xu, X., Liu, X., Wu, X., Wei, L., & Zhang, Y. (2014). ATP1A3 mutations and genotype-phenotype correlation of alternating hemiplegia of childhood in Chinese patients. *PLoS One*, *9*(5), e97274. https://doi.org/10.1371/journal.pone.0097274

Zeisel, A., Hochgerner, H., Lonnerberg, P., Johnsson, A., Memic, F., van der Zwan, J., Häring, M., Braun, E., Borm, L. E., Manno, G. L., Codeluppi, S., Furlan, A., Lee, K., Skene, N., Harris, K. D., Hjerling-Leffler, J., Arenas, E., Ernfors, P., Marklund, U., & Linnarsson, S. (2018). Molecular architecture of the mouse nervous system. *Cell*, *174*(4), 999–1014. e22. https://doi.org/10.1016/j.cell.2018.06.021

Zhong, N., Zhang, R., Qiu, C., Yan, H., Valenzuela, R. K., Zhang, H., Kang, W., Lu, S., Guo, T., & Ma, J. (2011). A novel replicated association between FXYD6 gene and schizophrenia. *Biochemical and Biophysical Research Communications*, *405*(1), 118–121. https://doi.org/10.1016/j.bbrc.2011.01.005

Zlokovic, B. V., Mackic, J. B., Wang, L., McComb, J. G., & McDonough, A. (1993). Differential expression of Na,K-ATPase alpha and beta subunit isoforms at the blood-brain barrier and the choroid plexus. *The Journal of Biological Chemistry*, *268*(11), 8019–8025.

SUPPORTING INFORMATION

Additional supporting information may be found in the online version of the article at the publisher's website.

How to cite this article: Jiao, S., Johnson, K., Moreno, C., Yano, S., & Holmgren, M. (2022). Comparative description of the mRNA expression profile of Na^+/K^+-ATPase isoforms in adult mouse nervous system. *Journal of Comparative Neurology*, *530*(3), 627–647. https://doi.org/10.1002/cne.25234